Electron tunneling measurements on pure bulk thorium

by

Brent Alan Haskell

A Dissertation Submitted to the

Graduate Faculty in Partial Fulfillment of

The Requirements for the Degree of

DOCTOR OF PHILOSOPHY

Major Subject: Solid State Physics

Approved:

Signature was redacted for privacy.

In Charge of Major Work

Signature was redacted for privacy.

Head of Major Department

Signature was redacted for privacy.

Dean of Graduate College

Iowa State University
Of Science and Technology
Ames, Iowa

1971

TABLE OF CONTENTS

INTRODUCTION

A comprehensive theory of superconductivity must account for a number of specific phenomena, among them the Meissner effect ($\underline{B=0 \text{ within a}}$ superconducting body), zero electrical resistance, the dependence of the transition temperature upon isotopic mass, a second-order phase transition at the critical temperature (in zero magnetic field), and the existence of an energy gap for single particle-like excitations.* The theory proposed by Bardeen, Cooper, and Schrieffer (hereafter BCS) (1) in 1957 was able to account for all of the above phenomena, as well as to provide a surprisingly good fit to existing experimental data.

The BCS theory is based on the idea that phonons (lattice vibrations in a crystal) can mediate an attractive interaction between electrons. The BCS theory assumes Bloch individual particle wave functions for normal state electrons; the specific model treated by BCS assumes a constant interaction energy between the electrons and as such applies specifically to single conduction band, isotropic superconductors. The superconducting state is a special combination of Bloch states in which pairs of electrons with opposite momenta and spin continuously make use of the electron-phonon interaction to form a coherent state which is lower in energy than the normal state.

A very striking feature of the microscopic theory is the prediction of an energy gap in the excitation spectrum. The existence of such a gap had been suggested by measurements of the electronic specific heat (2).

---

*It should be noted that only the simpler superconductors display all of the phenomena listed.

At sufficiently low temperatures, the presence of an energy gap would cause the specific heat to be dominated by a Boltzmann factor. The data then would have an exponential dependence in that temperature region with the argument of the exponential being directly related to the value of the energy gap.

Energy gap behavior also had been observed by Richards and Tinkham (3) using far infrared radiation as a probe. They found that the absorption was zero until the photon energy of the incident radiation became equal to the energy gap. The absorption then rose rapidly to the normal state value with increasing photon energy.

One of the most sensitive measurements of the energy gap is obtained via the technique of electron tunneling. Frenkel (4), in 1930, was the first to suggest an experimental tunneli configuration; however, it was not until three decades later that Giaever and co-workers performed the first tunneling experiments (5,6,7). Tunneling is a quantum mechanical effect which is related to barrier penetration. When a classical barrier has an extent which is less than that of an electronic wave function, a finite probability exists that the electron will be found on the opposite side of the barrier, i.e., that it will have "tunneled" through the barrier. In the abovementioned experiments the classical barrier consisted of the oxide of a metal, so that the tunnel junction was of the form metal-metal oxide-metal. The authors argued that if one or both of the junction constituents was a superconductor, any observed changes in the tunneling current as a function of applied voltage would be the result of a change in the superconducting density of states of the metals. The

strength of the tunneling technique lies in the fact that it provides a measure of the reduced single particle density of states, from which information about the superconducting energy gap can be obtained.

Bardeen (8), and Cohen, Falicov, and Phillips (9) have used different approaches to demonstrate that there is indeed a one-to-one correspondence between measured differential conductance curves and the superconducting density of states, although the two are equal only at T=0. For non-zero temperatures, differential conductance curves include kT thermal smearing, and Clem (10) has discussed this relationship between the superconducting density of states and measured differential conductance curves.

The early tunneling measurements were done on metals which formed acceptable oxides and which were easily evaporated, namely lead, tin, aluminum, and indium (11,12). Agreement with the BCS theory was good, although small discrepancies existed. Deviations from BCS theory had been found for photon absorption data (13), as well as specific heat data, and it was suggested that the energy gap was anisotropic over the Fermi surface (14). In conjunction with this, the suggestion also was made that two gap energies, one large and one small, might provide an explanation for experimental deviations from BCS predictions (15).

The notion of two energy gaps was introduced by Suhl, Matthias, and Walker (hereafter SMW) (15) in an extension of the BCS theory to the case where two bands of electrons in a metal overlap. In their paper they follow the BCS approach, but include in their Hamiltonian an interaction energy between electrons in different energy bands, as well as energy terms for electrons interacting within one band. The interaction energies

are labelled V_{sd}, V_{ss}, and V_{dd}, where the subscript s (d) denotes s-like (d-like) electrons. The calculation leads to the existence of an energy gap corresponding to each band. In the limit of zero interband coupling (V_{sd}=0), there appear two energy gaps and two distinct transition temperatures unless $N_s V_{ss} = N_d V_{dd}$, where N_s and N_d are the densities of states of the s and d bands. In the case of weak interband coupling, only one transition temperature can exist, although two energy gaps are still evident. In the limit of very strong interband coupling, the smaller energy gap merges into the larger one when N_s=N_d, leaving only one gap with a BCS-like temperature dependence, while for N_s not equal to N_d two energy gaps still exist. For moderately strong interband coupling, the smaller gap lies between the strong and weak interband coupling cases and depends upon the specific value of V_{sd}. Figure 1 illustrates the cases discussed above.

Garland also has considered the effect of multiple bands on superconducting properties (16). He assumes that the Fermi surface is separable into distinct s and d regions. For the case of a "clean" superconductor, different and partially decoupled energy gaps should exist, both of which could be anisotropic. In this "clean" case, he predicts anomalies in the temperature-dependent critical field and specific heat curves. Such anomalies should be observable experimentally.

Garland also finds that mixing of the s and d wave functions, as in the case of an impure sample, causes evidence of a second gap to disappear. He terms the impure case the "dirty" limit and maintains that very few, if any, two band metals have been sufficiently purified to permit

observation of the second gap. However, no experimentally usable criterion exists for distinguishing between "clean" and "dirty" samples. Garland has used the definition of Anderson (17), who has taken the dividing line between the two classes to be that point at which the electronic mean free path is equal to the coherence length. It is not known whether this condition for a clean sample is required if separate energy gaps are to be observed.

Many of the transition metals show evidence of being two-band superconductors. In the following, a transition element will be taken as one which has completely filled or empty f shells, and partially filled d shells. The valence electrons are of s-type and d-type, with the d electrons being bound more tightly so that they have considerably more localized wave functions than the loosely bound s electrons. Because of the localization of the d electrons, the density of states for them will be relatively high. Therefore, in these metals N_d usually is assumed to be much greater than N_s, where again N_d (N_s) is the density of states of d (s) electrons. Many theories approximate the ratio N_s / N_d by zero. For the same reasons, the d electrons usually are assigned a much higher effective mass than the more mobile s electrons.

It long has been understood that the overlap of s and d bands in the transition metals leads to an increased normal state resistivity (18). This effect, which is due to the band overlap, occurs when s electrons (which are more mobile and therefore are the primary carriers of current) are scattered into vacant d sites where their contribution to the conductivity is diminished. At low temperatures the resistivity can be strongly

affected by electron-electron scattering, again due to very high d band density of states at the Fermi level. This predicts a T^2 dependence for the low temperature resistivity, and a marked shift from the normal T^5 law is expected and observed for many transition elements (18). Deviation from the low temperature T^5 law can be taken as an indication of overlapping bands.

Wilson (19) has calculated the temperature dependence of the electrical resistivity due to s-d scattering. This scattering occurs when an s electron is scattered into the d band by a phonon (and is effectively trapped there by the high density of states). At low temperatures this effect will depend upon the number of phonons available and will vary as T^3, while at very low temperatures (say $T < \theta_D/40$, where θ_D is the Debye temperature) the effect begins to drop away exponentially with temperature. Webb (20), in his work on niobium, found that the T^3 term provided the dominant contribution to the resistivity from just above the transition temperature to about 50 K.

There are experimental indications that superconductivity in the transition metals is not caused solely by the electron-phonon interaction. Prominent among these indications is the absence or considerable reduction of the isotope effect in these metals (21). Garland (16) considered three possible mechanisms for superconductivity in the transition metals: 1) the intraband screened Coulomb interaction between s electrons, 2) intraband interactions arising from the exchange of virtual phonons, and 3) an attractive effective interaction arising from the small coupling terms between the s and d band gap equations. His calculations led to the

existence of an attractive interaction between s electrons due to screening by the s-d electron cloud. However, the theory predicted a first-order transition at the transition temperature and an energy gap much larger than exists. Peretti (22) calculated a similar interaction between s electrons and found it to be attractive. His calculations yielded an appropriate magnitude for the energy gap, the absence of an isotope effect, and a second-order transition. Although the issue is not settled, it may be that superconductivity in the transition metals is not due strictly to the electron-phonon interaction. This being the case, one should not be disturbed if the transition metals show experimental deviations from the predictions of the BCS theory.

Direct indications of multiple band behavior in the transition elements are available. Shen, Senozan, and Phillips (23) measured the specific heat of single crystal samples of niobium, tantalum, and vanadium. Their niobium data deviated sharply from the BCS prediction at low temperature, but could be explained using a two energy gap scheme. The tantalum and vanadium samples showed similar behavior, though not as pronounced as with the niobium. Later, Sung and Shen (24) calculated the specific heat curve using a SMW model and were able to fit the above data to their calculations. They also calculated the effect of non-magnetic impurities but were unable to fit the experimental data with their results. They postulated that the electronic structure of transition metal impurities had to be taken into account to explain fully the experimental data.

Radhakrishnan (25) calculated the penetration depth as a function of temperature using the two band model. He was able to fit data for niobium

by using parameters which Shen et al. had deduced. He also used the same model to calculate the upper critical field (26); he again obtained a reasonable fit to existing niobium data.

The thermal conductivity of single crystal niobium has been measured by Carlson and Satterthwaite (27). They were able to explain anomalous results in terms of a two gap model, but with different values from those of Sung and Shen for the energy gap and relative density of states of the second band. Tang (28) has pointed out that this analysis assumed that interband interactions were zero, a generally unreasonable assumption. Tang was able to correct the Carlson and Satterthwaite analysis to achieve better agreement with Sung and Shen.

In all of the results for niobium, the second energy gap $2\Delta_s$ was much smaller than the larger one $2\Delta_d$, with $\Delta_s / \Delta_d \sim 1/10$, and $N_s / N_d \sim 10^{-2}$. The fact that nearly all of the experimental evidence for a second energy gap relates to niobium is at least partly due to the high transition temperature of niobium. The high T_c allows experimental access to very low reduced temperatures.

Sung and Wong (29) have calculated the effect of impurities in the two band model. In the limit $N_s \ll N_d$ their results show that the d band properties are essentially unchanged by the addition of impurities, but that the properties of the s band are highly sensitive to impurity concentration. The effect of impurities is to increase the magnitude of the energy gap associated with the s band. These authors also point out that N_s and N_d are determined by the area of the Fermi surface covered by the separate bands.

One would expect that energy gap anisotropy should be observed in electron tunneling measurements. Zavaritskii (30) studied the energy gap of tin and noted a significant variation in Δ, the superconducting energy gap parameter, with crystallographic orientation. He then did a fairly exhaustive study of Δ as a function of orientation and attempted to relate his results to the features of the Fermi surface of tin. The results were not conclusive, although apparent correlations exist between his data and parts of the tin Fermi surface. He suggested that a multiple gap model might help to explain his data.

MacVicar and Rose (31) observed structure in single crystal niobium tunneling data which they interpreted as evidence of a possible second gap. Similar structure had been previously observed by Giaever (32), Townsend and Sutton (33), and Sherrill and Edwards (34), but had been attributed to impurities or other sample imperfections. Further work by Hafstrom, MacVicar, and Rose (35,36,37) has pointed more strongly to the existence of a second gap in high purity single crystal niobium. Generally reproducible structure was obtained and related to the general features of the niobium Fermi surface (as calculated by Mattheiss (38)). In addition, Shen observed structure in tantalum tunneling experiments (39) which could be due to the presence of a second energy gap.

The exact selection rules which govern the tunneling process are not yet firmly established. A selection rule which often is used conserves the group velocity of the electron normal to the barrier. Using this rule, Clem (40) has shown that, for a metal-barrier work function of 1 eV and an oxide thickness of 20 $\mathring{A}$, 95 percent of the tunneling current is carried by

electrons whose momenta arewithin 10 degrees of the normal to the barrier, and Bennett (41) maintains that all of the electrons which contribute significantly to the tunneling current have velocities within 5 degrees of the surface normal. Dowman, MacVicar, and Waldram (42) suggest that a more likely conserved quantity in tunneling is the k vector in the repeated zone scheme of the metal normal to the barrier. They point out that conservation of velocity normal to the barrier is not synonymous with their restriction on the normal k vector. A further complication is added by the fact that in both of the above selection rules different parts of the Fermi surface can contribute simultaneously to the tunneling current. However, the partial success of Dowman et al., and Zavaritskii, in the correlation of observed energy gaps with variations in the Fermi surface does indicate that the tunneling current in a given crystallographic orientation is substantially related to a specific part of the Fermi surface.

Tunneling into the transition metals long has been plagued with a number of experimental problems. Bulk samples are used almost without exception for these tunneling measurements, so that an oxide must be grown on their surface. In the transition metals a tunneling experiment samples the metal only within a small distance (as little as 100 Å) of the surface oxide (43), so surface purity is critical. Surface effects alone could explain the high failure rate in obtaining "good" tunnel junctions. The sampling depth for the tunneling electrons decreases with increasing dc bias (39) and this could explain why many transition metal tunnel junctions show acceptable characteristics in the region of the energy gap but are

almost devoid of phonon effects at higher biases.

A problem which exists for nearly all transition metal tunnel junctions is that of "excess currents" (37,39). Within certain limits (35), MacVicar takes data in spite of these "excess currents", which she postulates may be due to tiny shorts through the junction oxide. Marcus (44) also has proposed the existence of metallic junction shorts as an explanation for subharmonic structure in two-superconductor junctions.

The presence of zero-bias anomalies presents further difficulty with transition metal tunneling (45). The zero-bias anomaly is an increase in conductance, centered about zero bias, which can be attributed to the presence of magnetic impurities in or close to the oxide region (46). The anomaly is temperature-dependent and presumably not related to the density of states of the superconductor.

One would expect thorium to be very similar to the transition metals. Gupta and Loucks (47) have calculated the electronic structure of thorium by the relativistic augmented-plane-wave method and have concluded that thorium and other of the lighter actinides are similar to the transition metals and can be described by the same s-d energy band model. Thorium, the first of the actinides, is an fcc metal with valence 4. The valence electrons are $6d^2$ and $7s^2$, making the metal consistent with our previous definition of a transition metal. With a melting point of 1800 ^{o}C and a low vapor pressure, thorium is an extremely difficult metal to evaporate. It is not known whether thorium shows an isotope effect, since only one abundant stable isotope exists.

A number of low temperature experimental measurements have been

performed on thorium. Among those which are pertinent to our work are low temperature susceptibility and specific heat (48), resistivity (49), electronic structure by the de Haas-van Alphen effect (50), thermal conductivity (51), superconducting critical field (52), and anisotropy of the superconducting energy gap (53). These measurements will be discussed in the following pages.

Gordon et al. (48) measured the specific heat of thorium and found a ratio at the transition temperature of $C_{es}(T_c) / \gamma T_c = 2.42$, which is very close to the BCS value of 2.426. Their data did not extend below 1 K for the superconducting phase, so no evidence of a smaller gap should be expected. They deduced a number of experimental parameters from their data and concluded that thorium was a surprisingly ideal superconductor.

Decker and Finnemore (52) calculated a number of experimental parameters for thorium based on critical field measurements. They obtained the value $2\Delta(0) / kT_c = 3.53$, in good agreement with the BCS prediction. The critical field curve is within 0.3% of the BCS prediction at all temperatures, although a slight systematic deviation from BCS can be observed. In spite of the general agreement with BCS predictions for their samples, the authors feel that the closeness of fit to BCS is probably fortuitous and that the effect may be the result of strong-coupling effects just cancelling anisotropy effects (40).

Anderson, Peterson, and Finnemore (53) found that thorium is an anisotropic superconductor with a value of the mean-square anisotropy constant $\langle a^2 \rangle = 0.021$, as determined by a fit of their data to the theory of Markowitz and Kadanoff (54). However, the critical field data of Decker and

Finnemore lie above the calculated curve corresponding to this measured anisotropy constant. The discrepancy again could be caused by strong-coupling effects (40).

Measurements of the thermal conductivity of thorium by Cappelletti and Finnemore (51) were analyzed in terms of the theory of Bardeen, Rickayzen, and Tewordt (55), which is based on a BCS model. Their data for K_{es}/K_{en}, where K_{es} and K_{en} are the superconducting and normal electronic thermal conductivities, lie above the Bardeen et al. predictions for reasonable assumptions about the phonon contributions. This result is expected for an anisotropic superconductor, since portions of the Fermi surface with a small gap tend to dominate the low temperature thermal conductivity. Assuming no scattering of the electrons by phonons, the closest fit to their data is obtained for the value $2\Delta(0)/kT_c = 3.15$.

Peterson et al. (49) have measured the resistivity of very pure thorium. Below 80 K the data can be fit to the Bloch-Grüneisen function with a Debye temperature of 135 K (this value is lower than the value of approximately 165 K usually obtained for thorium). At higher temperatures the data rise above the Bloch-Grüneisen prediction for θ_D equal to 135 K. At low temperatures, $T/\theta_D < 1/6$, the resistivity data deviate from a single conduction band T^5 dependence. The best fit was for a $T^{3.5}$ behavior, and it will be recalled (see page 6) that this type of deviation is indicative of two-band structure.

The calculations of Gupta and Loucks (47) have been confirmed by the experimental results of Boyle and Gold (50). The calculated Fermi surface of thorium is shown in Figure 2. There are three distinct segments of the

surface: 1) a hole surface at the center of the Brillouin zone shaped like a rounded cube, 2) hole surfaces on the symmetry lines ΓL shaped like dumbbells, and 3) electron surfaces on the symmetry lines ΓK shaped like pairs of lungs. It is readily seen that the Fermi surface varies markedly with crystallographic orientation, and one should expect energy gap anisotropy in thorium. Gupta and Loucks also mention that the cubical section of the Fermi surface is of special interest because the opposite faces of such figures can "nest" into one another. Such "nesting" might result in phonon and magnon spectra anomalies, or an influence on the arrangements of any impurity magnetic moments present in the metal (47). It is interesting to speculate about whether such an effect might be related to the non-magnetic behavior of cerium when it is dissolved in thorium (56).

While thorium conforms to the predictions of the BCS model in many ways, there clearly are deviations which remain unexplained. We therefore have undertaken to perform tunneling experiments on thorium, in spite of the difficulties inherently associated with tunneling into transition metals. The results are expected to contribute to our present understanding of the metal thorium.

EXPERIMENTAL DETAILS

Introduction

Electron tunneling data in this experiment were obtained as X-Y recorder plots of di/dv vs v, where i represents the current through the tunnel junction, and v represents the voltage across it. The data are used to obtain information about the reduced density of states of the samples according to the following relationship for σ, the normalized tunneling conductance:

$$\sigma = \frac{(di/dv)_{ns}}{(di/dv)_{nn}} , \qquad (2\text{-}1)$$

where the subscript ns indicates a normal metal-superconductor tunnel junction.

The data were taken in a He-3 refrigerator shown in Figure 3 (the glass double Dewar system, liquid helium inner and liquid nitrogen outer, is not shown), the operation of which is relatively simple. He-4 condensed into the He-4 reservoir is cooled by pumping on this liquid with a vacuum pump to obtain temperatures near 1 K. He-3 then is condensed into the He-3 reservoir (or pot) and cooled similarly to obtain temperatures as low as 0.28 K. The higher vapor pressure of He-3 permits cooling below the lowest temperatures obtainable with He-4 alone.

Two types of tunnel junctions were measured, one type being a double thin film junction, and the other being a single film on top of a bulk sample. A double thin film junction is prepared by first evaporating

a metal film onto a glass substrate, oxidizing it by exposure to air, and then evaporating a second metal film at right angles to the first one. The tunnel junction consists of the region where the two films overlap. A bulk sample tunnel junction is prepared by first cleaning the surface of a bulk sample, letting that surface oxidize, masking the surface in such a way as to leave only a narrow strip exposed, and then cross-evaporating a thin film. The tunnel junction is the region of overlap between the exposed strip of sample and the thin film.

The double thin film junctions were prepared in order to learn the technique of film evaporation, and were measured in order to check the operation of the electronic detection system. The bulk sample junctions were prepared on bulk thorium because the metal is extremely difficult to evaporate.

The bulk thorium samples were cleaned in high vacuum by electron bombardment, were oxidized in situ in pure oxygen, and were masked by painting the surface with Collodion. The tunnel junctions were completed by cross-evaporation of a gold or silver film.

The electronic detection system is capable of measuring both di/dv and d^2i/dv^2. The second derivative is used primarily to observe phonon effects on the density of states, which are small and appear at voltages greater than the energy gap. Our junctions were such that phonon effects could not be observed and comments pertaining to d^2i/dv^2 will be offered solely in the interest of completeness.

The tunnel junctions were measured as part of one arm in a bridge circuit. The bridge was balanced at one point and as the characteristics

of the junction changed with the bias voltage across it an operational amplifier provided voltage to a feedback loop which acted to maintain the original balance condition. As will be shown, the feedback voltage from the operational amplifier is proportional to di/dv for the junction. This feedback voltage is sent to a lock-in amplifier whose dc output is proportional to the amplitude of the feedback voltage. The output of the lock-in amplifier is sent to the Y axis of the X-Y plotter, where it is recorded as a function of applied dc bias voltage across the tunnel junction.

Cryostat

The data were taken over the temperature range 0.3 K to 1.5 K using the He-3 refrigerator shown in Figure 3. The details of operation of such a system have been discussed elsewhere (57), and only comments particular to this experiment will be included here.

Shortly before the first data were taken, the He-4 reservoir (or pot) was rendered inoperative by a block in the pumping line leading to it. The behavior of the system indicated that the block was at the top of the He-4 pot, and it was assumed to be in the small orifice there. After a number of different attempts failed to unplug the line, it was decided to forego immediate repair in favor of obtaining data. The He-3 system therefore was operated (in the case of all the data reported in this manuscript) by pumping on the liquid helium in the helium Dewar and letting this bath serve as a replacement for the He-4 pot.

The sample was mounted vertically on a small copper block which was directly connected to the He-3 pot. A single layer of Kimwipe was used for electrical insulation, and GE7031 varnish was used to hold the sample

in place and to provide thermal contact between the sample and the copper block. There were no indications that such an arrangement was not satisfactory.

The electron tunneling measurements were made by means of a bridge technique, and it was desirable to keep the resistance of the tunnel junction leads as low as possible. This was accomplished via the combined use of copper and lead-coated manganin wires. The excellent thermal conductivity of copper prohibits the sole use of copper leads, since they would allow excessive heat conduction into the sample from warmer parts of the cryostat. The lead-coated manganin wire consisted of a 0.0005 in. coating of lead on 0.006 in. diam manganin wire. Below the superconducting transition temperature of lead (where all the data were taken) the electrical resistance of the lead is zero, and the thermal conductivity of the lead plus manganin is substantially lower than that of copper wire of a reasonable size.

All electrical leads ran from a terminal strip at room temperature to one of two terminal boards located just above the vacuum can (in the helium bath). The leads entered the vacuum can through nylon-epoxy seals (58). The lead-coated manganin junction leads extended 30 cm inside the vacuum can where they were joined to No. 36 copper wires which were immediately anchored to the base of the He-3 pot with GE7031 varnish; they then dropped to a final terminal board where they made solder contact to the leads attached to the junctions. The leads to the germanium resistance thermometer, the carbon resistance thermometer, and the sample heater were of manganin wire. Once inside the vacuum can, these leads were thermally

anchored at both the He-4 and He-3 pots with GE7031 varnish. The carbon thermometer and sample heater leads were connected to those elements immediately, while the germanium thermometer leads were anchored again to the He-3 pot before connecting to the thermometer.

The heat leaks down the leads were relatively small for the above configuration. The estimated heat leak due to one of the manganin leads was 5 nW, while the total heat leak into the sample from the junction leads was estimated to be less than 5 μW. The radioactive self-heating of the thorium was another possible heat input to the sample, but it was estimated to be 10 nW, and thus insignificant by comparison to heat leaks down the leads.

Regardless of the estimated heat conductivity down the leads, accurate thermometry demands that the leads attached to the germanium thermometer be thermally anchored to a point at common temperature with the sample. Following Swenson (59), copper strips were bonded to the same copper block which supported the sample. The strips were electrically insulated from the block by a thin nylon mesh and were cemented in place with Armstrong A-6 epoxy. The manganin wires and the thermometer leads were soldered to opposite ends of these strips, thus providing a heat sink to absorb any heat energy flowing down the manganin wires.

Temperature Control and Thermometry

Once the helium bath was pumped down to a temperature slightly above that at which the data were to be taken, He-3 was condensed into the He-3 pot, and the temperature of the junctions was controlled by pumping on the liquid in the He-3 pot through a fixed system of valves, while

simultaneously counteracting the cooling effect by supplying power to a 50 Ω manganin heater. The temperature control circuit used a 3-wire (lead compensated) Wheatstone bridge in which the resistance of a Speer carbon resistor (labelled SR-2) was balanced against a decade resistance box. The imbalance voltage was amplified by a Keithley 153 microvoltmeter and sent to a transistor-controlled heater power supply which turned the heater current on or off whenever the SR-2 resistance became greater or smaller than that of the decade box. When the regulating system was operating properly and equilibrium had been reached, it was possible to maintain the temperature constant to within ± 2 mK for periods of thirty minutes or longer.

The resistance of the germanium thermometer, GR1592, was obtained from measurements of the voltage drops across the thermometer itself and across a standard resistor contained in the thermometer current loop. The measuring currents through GR1592 were 10 μA for temperatures above 1 K (approximately) and 1 μA for lower temperatures. The voltages were measured with an approximate uncertainty of 0.2 μV using a Leeds and Northrup Type K-3 Potentiometer and a Hewlett-Packard Model 419A DC Null Voltmeter. This corresponded to a temperature uncertainty of about 2 mK at 1.4 K where the thermometer resistance and its temperature derivative were at a minimum for the temperature range of interest. The thermometer resistance increased as lower temperatures were obtained, and therefore the temperature uncertainty decreased as well.

The resistance thermometer GR1592 was calibrated previously by Prof. D. K. Finnemore of this laboratory over the temperature range 0.3 K to

4.2 K using paramagnetic salt thermometry below 2 K and He vapor pressure thermometry above 1.6 K (60). The R vs T values from this calibration were fit to an equation of the form

$$(\ln T) = \sum_n Q_n (\ln R)^n \qquad (2\text{-}2)$$

by minimizing the expression

$$S = \sum_k \{ \ln T - \ln T_{cal} \}_k^2 \qquad (2\text{-}3)$$

in the least squares sense. The criteria for a good fit were that $(T - T_{cal})$ should be small for all data points, and that (dR/dT) and (d^2R/dT^2) for the calculated curve should be smoothly varying. A fourth order fit was chosen for the temperature range 0.3 K to 2.0 K with the standard deviation from the calculated curve being 2.4 mK. The fit constants are given in Table 1.

Table 1. The fit constants for germanium thermometer GR1592

	0.3 to 2.0 K
Q(0) =	$0.14695191145520 \times 10^{2}$
Q(1) =	$-0.59978171470915 \times 10^{1}$
Q(2) =	$0.89901486460550 \times 10^{0}$
Q(3) =	$0.62347704137502 \times 10^{-1}$
Q(4) =	$0.15691061867330 \times 10^{-2}$

Carbon resistor SR-2 was used as a secondary thermometer as well as a temperature control sensor. The calibration of carbon resistors can vary by a few percent when cycled between room and liquid helium temperatures, and if they are used as primary thermometers they must be recalibrated at a few points during each low temperature run. GR1592 was inoperative in the case of one tunnel junction (Au on Th No. 1), and for that case the recalibration of SR-2 was done against the vapor pressures of liquid He-4 and liquid He-3.

Sample Preparation

It will be recalled that the double thin film tunnel junctions consisted of a metal film which had been cross-evaporated over another oxidized metal film. The substrates used for these junctions were glass microscope slides which were fire-polished before use. Electrical leads were inserted into indium blobs which had been placed on the substrate with a soldering iron heated just above the melting point of the indium. Metals were evaporated by resistively heating tungsten filament baskets inside a conventional bell jar evaporation system (see Figure 4). The bell jar was pumped to a vacuum or 10^{-5} Torr, or better, by a modified Cenco Model No. 93422-17 3 in. diffusion pump. The evaporation chamber was separated from the diffusion pump by both a cold trap and a baffle valve.

The bell jar was pumped to a roughing vacuum through a line which bypassed the diffusion pump, cold trap, and baffle valve. There was a danger of introducing pump oil into the bell jar if the initial pumping rate was great enough to cause vigorous back-streaming of the pump oil. A compromise therefore was necessary to ensure rapid evacuation of the

evaporation chamber, while simultaneously keeping pump oil back-streaming to a minimum. There were no indications that junction properties were affected by the procedure used to evacuate the bell jar.

The thin film junctions were all of the form Al-Al_2O_3-Metal. The aluminum was evaporated first, after which the film was removed from the bell jar and oxidized in a small oven which had been heated to approximately 100 ^{o}C. The oxidation time varied between 30 and 60 seconds, and during this time a second metal was placed in the evaporator in another tungsten basket.

All film evaporations were masked by a piece of aluminum sheet into which had been cut two 1 mm wide slits, separated by a distance of 6 mm, thereby providing for the concurrent preparation of two junctions. The mask was supported by four 10 cm long steel rods so that a typical boat-to-substrate distance was 8 cm.

The tunneling measurements on pure thorium were done on samples provided by Prof. D. T. Peterson of this laboratory. The pure thorium is obtained via the magnesium reduction of thorium tetrachloride, after which it is arc-melted into an ingot and further purified by electron-beam melting (61). This process is extremely consistent and the analysis of the resulting pure thorium varies only slightly with different batches. The analysis of one of the samples used in this experiment is given in Table 2.

The high vacuum system in which the thorium was processed was constructed of stainless steel and was equipped with an Ultek Model 20-092 100 liter/sec vac-ion pump. The system is illustrated in Figure 5. A detailed discussion of the operation of the high vacuum system has been given

by Stromberg (62), and only pertinent details will be presented here.

Table 2. Typical chemical analysis of pure thorium (impurity concentrations are given in ppm by weight)

Impurity	Concentration	Impurity	Concentration
C	46	Mn	< 20
O	122	Ni	< 5
N	22	Si	< 20
Al	< 20	Ta	Nd[a]
Ca	< 30	Ti	Nd
Cr	< 20	W	Nd
Fe	< 6	Y	Nd
Mg	< 20	U	< 0.9

[a]Nd - Not detected

The vac-ion pump could not operate continuously at pressures above 10^{-5} Torr; this made it necessary to reduce the pressure to that point by external means. A conventional Welch rotary pump was connected through a liquid nitrogen-cooled copper line to produce a roughing vacuum which was reduced further by means of an Ultek sorption pump. After the ion pump started, the system was baked for 12 to 24 hours at 250 ^{o}C to remove gases which had adsorbed onto interior surfaces of the system. The filament (to be described later) was outgassed for 4 to 6 hours, after which the sample was heated in a vacuum no worse that 4×10^{-8} Torr. The best vacuum obtained during sample preparation was approximately 2×10^{-9} Torr.

The thorium samples were received in sheet form with typical

dimensions in mm of 1 x 12 x 12. A small hole was drilled in one corner of the sample and it was mounted in the electron bombardment assembly as shown in Figure 6. The filament was made of 0.010 in. tantalum wire. The electrodes were made of 0.060 in. tungsten rod, with the exception of the lower part of the sample electrode, which was of similar size tantalum. Connections between dissimilar materials were made by spot-welding, although the sample itself was tied in position with 0.010 in. tantalum wire, and not spot-welded.

After the apparent ultimate vacuum had been obtained, the filament current was reduced to its operating value of approximately 4 A. A positive voltage was applied to the sample, and electrons emitted from the hot filament were accelerated to the sample surface. The accelerating voltage used varied from 1000 to 1400 V, depending upon such factors as the surface area of the sample and the proximity of the filament to the sample. The emission current (from filament to sample) was typically 60 mA, so that the power input to the sample was approximately 60 to 85 W.

Sample temperatures during preparation were estimated by visual comparison with the color scale of temperature (63), as well as with an optical pyrometer. At the power levels stated, the sample temperature was estimated to be approximately 1000 to 1400 ^{o}C. The sample was held at these temperatures for more than two days in most cases.

Recrystallization in thorium begins to occur above 800 ^{o}C. Thus, the sample preparation procedure in this experiment accomplished three objectives: 1) the sample was outgassed and purified at elevated temperatures while under high vacuum, 2) the sample surface was cleaned by sublimation,

and 3) the sample was annealed in high vacuum at temperatures well in excess of the recrystallization temperature. During recrystallization, regions of single crystal tended to form, so that in most cases the thorium side of the tunnel junction consisted of a region which was wholly or partly single crystal.

Visual appearance of the sample was the criterion which was used to decide when it was time to remove the sample from the high vacuum system, since during bombardment the sample surface gradually took on the look of an extremely well-polished metal. In many cases it was possible to see what were taken to be the grain boundaries of the single crystal regions mentioned above.

Once the sample was ready for the preparation of the tunnel junctions, it was allowed to cool for a period of 15 to 20 min before it was oxidized in situ. Oxygen was bled into the system until the pressure increased to approximately 0.1 atm. This pressure was maintained for a period of 25 min, after which time the oxygen pressure was increased to atmospheric and the sample was removed. The sample remained in the full oxygen atmosphere for approximately 5 min before it was exposed to air because four vacuum flange bolts had to be removed prior to removal of the sample.

The purpose of the above oxidation procedure was to create a uniform oxide layer approximately 20 Å thick which hopefully would prohibit further rapid oxidation when the sample was introduced to air. Air was used in the first attempts at oxidation and water vapor in the air was blamed for catalyzing the excessive oxidation which occurred.

Shen has prepared tantalum samples for tunneling measurements by a

process similar to the one used here (39), but he oxidized his samples at 50 °C for 3 hours in a stream of oxygen. When we used this oxidation procedure with thorium, the tunnel junctions exhibited a resistance greater than 100 kΩ, indicating that the oxide layer was prohibitively thick. Only high resistance junctions were obtained as well when the pressure exceeded 0.1 atm in the normal oxidation procedure.

Upon removal from the high vacuum system, the sample was disconnected from the electron bombardment assembly, two indium solder contacts were made to the thorium, and fine copper leads were soldered into place. The best contacts to the thorium were achieved when the soldering iron was held at a temperature only slightly above the melting point of the indium.

After the leads were attached to the thorium, the surface was painted with Collodion so as to leave an exposed strip of oxidized thorium 1 to 2 mm wide which extended between the attached leads (see Figure 7). Collodion forms a very thin film when applied in this manner, and the most critical control of the masking procedure was achieved when the operation was performed under a microscope. Best results were obtained by using relatively fresh Collodion (no more than a few weeks old).

When the Collodion was dry, indium blobs were deposited on the Collodion and No. 36 copper leads were soldered into them. Lack of care during this step could cause the hot indium to burn through the Collodion and to short to the thorium. Usually such a fault could be remedied by removing the indium and locally patching the Collodion film.

The sample then was placed on the evaporation mask in the bell jar and evacuation was begun immediately. The total elapsed time between removal

from the high vacuum system and subsequent evacuation of the bell jar ranged from 15 to 45 minutes, depending on the dexterity and luck of the experimenter. The evaporation of the cross strips was not attempted until the bell jar vacuum had reached or passed 10^{-5} Torr. Such a vacuum was usually attained within 4 to 5 hours, although in many cases the system was allowed to pump overnight prior to evaporation. At all times, an adequate liquid nitrogen level was maintained in the cold trap.

The evaporation of the cross strips completed the formation of the tunnel junctions. Evaporation was continued until a visibly thick film had been deposited, or until the resistance of one of the junctions had reached a desirable value. Figure 7 illustrates the appearance of two completed tunnel junctions.

The resistance of a tunnel junction could be monitored during evaporation by means of the simple ac bridge shown in Figure 8. The bridge makes a two-terminal measurement, balancing the resistance and capacitance of the tunnel junction against variable standard values. An ohmic resistance yields a straight line on the oscilloscope display. A tunnel junction, even in the normal state of both metals, is not ohmic, and therefore the oscilloscope display is non-linear. A "good" junction is characterized by desirable values of resistance (approximately 100 Ω) and capacitance (about 0.025 μf), and by a non-linear trace on the oscilloscope.

Clip-on leads were connected to two junction leads and during evaporation the junction resistance was used as a guide for attaining the proper film thickness. The voltage output of the oscillator was kept very close to minimum value to ensure no electrical effect on the junction during

evaporation. Heretofore, junction evaporation had been a relatively blind process, but use of this bridge greatly increases the probability of obtaining a measurable junction. Use of the bridge also enables one to select for low temperature measurement only those junctions which have a good probability of being reliable.

Tunnel junction properties tend to change rapidly with time at room temperature. Therefore, as soon as an acceptable junction was obtained, it was mounted in the cryostat, the vacuum can was sealed, the system was evacuated, and the cryostat was immersed in liquid nitrogen. The junction usually reached 77 K within 1 to 2 hours and at that temperature junction properties remain stable. After the junction had reached 77 K and a good vacuum around the sample had been attained, the double Dewar system was installed and the sample was cooled to 4.2 K. Tunnel junctions usually remained stable for many days at liquid helium temperatures.

Electronics

The data obtained in this experiment were di/dv vs v traces from an X-Y recorder. The measurements were made by applying an ac signal to the tunnel junction and using harmonic detection techniques to measure di/dv (and if desired, d^2i/dv^2).

If a small ac modulation voltage (frequency ω, amplitude m) is applied to the tunnel junction which is biased at dc voltage v_o. then due to the non-linearity of the junction, the current through it can be expanded in a Taylor series:

$$i(v) = i(v_o) + (di/dv)_{v_o} m \cos \omega t + \frac{1}{2}(d^2i/dv^2)_{v_o} m^2 \cos^2 \omega t + \ldots . \quad (2\text{-}4)$$

Also, from simple trigonometry, one can replace $\cos^2\omega t$ by $\frac{1}{2}(1 + \cos 2\omega t)$. It is seen that, providing the modulation voltage amplitude m is constant, the component of junction current at frequency ω is proportional to di/dv and the component at frequency 2ω is proportional to d^2i/dv^2. It will be shown that, by considering the ac component of this current at frequency ω, a measure of $(di/dv)_{V_o}$ can be obtained.

The electronic detection system is illustrated in the block diagram in Figure 9. The key components of the system are the ac bridge (to be described below), one arm of which contains the tunnel junction, and the phase-sensitive detector (lock-in amplifier).

In the lock-in amplifier, the signal at the input terminals is sent through a narrow-band amplifier and then is mixed with a reference signal driven by the same oscillator. The output of the mixer is passed through an integrating RC time constant circuit thus providing a dc output signal proportional to the amplitude of the ac signal at the input to the lock-in device. Use of a lock-in amplifier has definite advantages over a tuned circuit: 1) the center of the pass band is determined by the reference frequency, 2) oscillator stability is not as severe a problem, since the center of the pass band is always locked to the signal frequency via the reference channel, so that if the input passband is not too narrow, a slight oscillator frequency drift introduces only a small phase angle change.

The lock-in amplifier provides high noise rejection, because of its extremely narrow over-all pass bandwidth. The main contributions to noise are white noise, which has a constant contribution per unit cycle

bandwidth, and flicker noise, which is inversely proportional to the frequency. The latter can be significantly reduced by using the oscillator at a frequency well above dc, and in this experiment the oscillator frequency was 1000 Hz. White noise voltage is proportional to the square root of the pass bandwidth and can be limited to some degree by reducing the pass bandwidth of the front-end amplifier in the lock-in device. However, if the bandwidth is made too narrow, this imposes increasing stability restrictions on the oscillator, thereby demanding that some compromise be made.

The schematic diagram for the tunneling bridge is shown in Figure 10. When measuring conductance (di/dv), frequency ω is used. Measurement of d^2i/dv^2 requires frequency 2ω, which is achieved by a frequency doubler circuit connected to the oscillator. It is also necessary to set the frequency input control on the lock-in amplifier to a value of 2ω.

In Figure 10 the junction leads are labelled i^-, v^-, i^+, and v^+. The resistance and the capacitance of the tunnel junction are balanced against R_d and C_d. C_d is a decade capacitance box and R_d consists of two 10-turn potentiometers connected in series. At balance, the input signal to the operational amplifier is zero, but as the tunnel junction characteristics change with dc bias an imbalance occurs and a voltage appears at the input to the operational amplifier. This voltage is amplified and current is fed back through the junction in such a way as to reduce the input difference voltage almost to zero. Thus, the feedback loop from the amplifier will operate to maintain a constant voltage across the tunnel junction (equal to the voltage across R_d). This constant voltage condition is the one

which permits us (see Equation (2-4)) to say that the component of the junction current at frequency ω is proportional only to di/dv. As will be shown below, the feedback current required to maintain the balance condition in the bridge is directly related to di/dv across the junction. The voltage producing this feedback current is sent to the lock-in amplifier and in turn its output is sent to the Y axis of the X-Y recorder.

A simplified form of the tunneling bridge is presented in Figure 11. We assume that the capacitance completely dominates the reactive part of the signal, so that $C_d=C_t$ balances the reactive part of the signal. The current i will be taken to consist only of ac contributions, and A is the amplification factor of the operational amplifier (A equals approximately 50,000 here). We can write the equation

$$e_o = A\,(iR_d - iR_t - \delta iR_t) \quad . \tag{2-5}$$

Also,

$$e_o = A\,(e_+ - e_-) = \delta i\,(R_f + R_t) + iR_t \quad . \tag{2-6}$$

Equations (2-5) and (2-6) can be combined to give

$$A\,\{\, i(R_d - R_t) - \delta iR_t)\,\} = \delta i\,(R_f + R_t) + iR_t \quad , \tag{2-7}$$

which can be solved for δi, yielding

$$\delta i = \frac{i\,\{\, R_t(-1 - A) + AR_d \,\}}{R_f + R_t + AR_t} \quad . \tag{2-8}$$

If we make the substitution

$$B = \frac{R_t}{R_f + R_t} \quad , \tag{2-9}$$

then Equation (2-8) can be written as

$$\delta i = \frac{iB \{ (-1 - A) + AR_d / R_t \}}{1 + BA} \quad , \tag{2-10}$$

$$= \frac{iBA}{1 + BA} \{ -\frac{1}{A} - 1 + \frac{R_d}{R_t} \} \quad . \tag{2-11}$$

The minimum value of BA was approximately 700, corresponding to a minimum value for R_t of 150 Ω (A = 50,000 and R_f = 10 kΩ), and therefore we can set BA/ (BA + 1) = 1. Since the conductance is the inverse of the resistance, we take $g_t = 1/ R_t$. Under these conditions Equation (2-11) can be written in the following form:

$$\delta i = i [R_d g_t - 1] \quad . \tag{2-12}$$

When the above expression for δi is substituted into Equation (2-6) and some slight rearranging is done, the following result is obtained:

$$e_o = iR_d R_f g_t + i (R_d - R_f) \quad . \tag{2-13}$$

It is seen from the above equation that the output voltage of the operational amplifier is linear with respect to the tunnel junction conductance g_t at frequency ω. The input signal to the lock-in amplifier and therefore the Y output of the X-Y recorder is proportional to the tunnel junction

conductance g_t. All of the data analysis was done in terms of the normalized conductance $\sigma = {}^{g}t_{sn} / {}^{g}t_{nn}$.

Since the output of the detection system is linear in conductance, and hence in di/dv, only two points are necessary to calibrate the Y axis of the X-Y recorder. One point, termed the "unity" level, is some point at which the tunnel junction is balanced by R_d and C_d. It is desirable that the balance at this "unity" level be unaffected by the energy gap structure of the superconductor. Therefore, this balance point is usually established in one of two ways: 1) for temperatures below T_c it can be established at a dc bias so large that all traces of energy gap structure have disappeared, or 2) for temperatures above T_c it can be established at zero dc bias. The second calibration point is taken with the junction removed from the circuit, corresponding to a value of zero conductance. Changes in the sensitivities of the lock-in amplifier and/or the Y axis of the X-Y recorder permit wide variation in the recorder deflection corresponding to a conductance change from the zero to the "unity" levels.

It should be noted that improper phasing of the lock-in amplifier can lead to spurious results caused by the contribution of reactive imbalance to the intended measurement of resistive variation. The experimental indication of a properly phased system is that a large reactive imbalance does not affect the resistive balance, and vice versa.

The dc bias sweep circuit can be seen in Figure 12, which is a schematic diagram for the entire electronic detection system. This bias circuit permits a linear sweep in time of the dc bias, as well as range and vernier controls. It is also possible to determine the starting position

for the sweep. The primary element of the bias circuit is another operational amplifier which acts as an integrator and permits the linear sweep in time. The output of the dc sweep circuit is fed to the junction and to the X axis of the X-Y plotter.

In low temperature measurements, it is desirable to keep noise levels below the level of kT thermal smearing. This kT smearing corresponds to 86 μeV per K, and therefore a measurement at 0.3 K imposes a noise level limit of about 25 μeV. The noise level due to a 1000 Hz signal at the junction is in the nanovolt region for resistances and detector bandwidths encountered in our measurements. A root-mean-square junction modulation voltage of 25 μV corresponds to a peak-to-peak modulation level of approximately 70 μV. Commonly applied modulation voltages were 30 to 50 μV peak-to-peak.

The conductance bridge was checked for linearity by replacing the junction with a decade resistor and parallel capacitor. Ten ohm leads were used to simulate the actual junction leads. The resistance was varied between 50 Ω and 10 kΩ and the bridge showed linearity to within the width of the recorder pen trace. Rogers (64) has done more extensive checks on an identical bridge. He found conductance linearity to within 0.1%, as well as stability to better than 1 part in 10^4 per hour. He estimated that the calibration procedure was accurate to about 1% for sample resistances between 100 Ω and 1000 Ω. In addition, he checked the effect of lead resistance changes on the output of the system. He found a fractional change in conductance of less than 3×10^{-4} per 1 ohm change in lead resistance.

THEORY

BCS Theory

The theory of superconductivity due to Bardeen, Cooper, and Schrieffer (BCS), along with many of its extensions, has been discussed in detail elsewhere (1, 65-67) and only a few of the basic ideas will be presented in this discussion. It was known that two electrons could experience an effective attractive interaction due to the mutual exchange of virtual phonons (68). When this attraction between the electrons is greater than their mutual Coulomb repulsion, bound pairs can be formed (69), and this notion is central to the BCS theory.

After assuming an attractive interaction between electrons, BCS formulated a wave function for the superconducting state which consisted of a linear combination of normal state configurations with individual particle Bloch states occupied in pairs of opposite momentum and spin. The wave function was of the form $\Psi(u_k, v_k)$, where u_k and v_k are variational parameters relating to the probability that the state k is occupied (v_k^2 is the probability that the state k is occupied, and u_k^2 is the probability that the state k is unoccupied). They minimized the free energy of the system with respect to the variational parameters and obtained the following relations for u_k and v_k:

$$u_k^2 = \frac{1}{2}\left(1 + \frac{\epsilon_k}{E_k}\right) , \tag{3-1}$$

$$v_k^2 = \frac{1}{2}\left(1 - \frac{\epsilon_k}{E_k}\right) , \tag{3-2}$$

where ϵ_k is the energy of an ordinary Bloch state measured from the Fermi energy, and E_k is given by the relation

$$E_k = (\epsilon_k^2 + \Delta_k^2)^{\frac{1}{2}} . \tag{3-3}$$

E_k represents the excitation energy required to create an unpaired quasi-particle in the state k. The quantity Δ_k is determined by the following self-consistency equation:

$$\Delta_k = \sum_{k'} \frac{V_{kk'}\Delta_{k'}}{2E_k} , \tag{3-4}$$

where $V_{kk'}$ is the magnitude of the attractive interaction energy. Δ_k is called the energy gap parameter and is equal to one half the value of the energy gap $2\Delta_k$.

BCS assumed an isotropic superconductor, so that $V_{kk'}$ is independent of k, and they defined $V_{kk'}$ by the following

$$V_{kk'} = V \qquad \text{for } | \epsilon_k | < \hbar\omega_c , \tag{3-5}$$

$$= 0 \qquad \text{otherwise} , \tag{3-6}$$

where ω_c is a cutoff value corresponding to a phonon frequency close to ω_D, the Debye frequency. They assume further that the density of Bloch states of one spin, N(0), remains constant over the region of interest and equal to the value at the Fermi surface. In the weak-coupling limit, the following expressions for the ground state energy and the energy gap parameter of the superconductor are obtained:

$$W = - 2N(0) \hbar^2 \omega_c^2 e^{-2/N(0)V} , \tag{3-7}$$

$$\Delta = 2\hbar\omega_c e^{-1/N(0)V} \quad . \tag{3-8}$$

It is also found that Δ goes to zero at a temperature $T = T_c$ given by the following relation:

$$\frac{2\Delta(0)}{kT_c} = 3.526 \quad . \tag{3-9}$$

One also can obtain the density of states for the quasi-particle excitations in a manner similar to that for a normal metal

$$\frac{\partial n(E_k)}{\partial E} = \frac{\partial n(\epsilon_k)}{\partial \epsilon}\frac{\partial \epsilon}{\partial E} = N(0)\frac{E}{(E^2 - \Delta^2)^{\frac{1}{2}}} \qquad \text{for } E \geq \Delta \ , \tag{3-10}$$

$$= 0 \qquad \text{for } E < \Delta \ , \tag{3-11}$$

where the expression for $\epsilon(E)$ is obtained from Equation (3-3), and $\partial n(\epsilon_k)/\partial \epsilon$ is the density of normal Bloch states at the Fermi surface, $N(0)$. One normalizes this expression with respect to $N(0)$ to obtain the normalized superconducting density of states, given by

$$n_s(E) = \frac{E}{(E^2 - \Delta^2)^{\frac{1}{2}}} \quad . \tag{3-12}$$

It is this density of states that electron tunneling measurements attempt to observe, as will be seen shortly.

The Suhl, Matthias, and Walker (15) model of a two-band superconductor assumes that the interaction energy between electrons can be different for different energy bands. This energy corresponds to the term $V_{kk'}$ in

Equations (3-4) through (3-6). They assume interaction energies V_{ss}, V_{dd}, and V_{sd}, which correspond to phonon emission and absorption by s-s, d-d, and s-d processes, respectively. A BCS approach is taken, with the interaction energies assumed constant and isotropic out to some cutoff point in the phonon spectrum, and with excitation energy relations similar to Equation (3-3) for both the s and d band energy gaps. Self-consistency equations are generated and solved (as in the BCS paper), and expressions for the energy gaps of the two bands are obtained.

As was previously mentioned, the limit $V_{sd} = 0$ yields two energy gaps and two transition temperatures (unless $N_s V_{ss} = N_d V_{dd}$) corresponding to curves A and A' in Figure 1. When V_{sd} is non-zero but small, the smaller energy gap takes the form shown by curve B and only one transition temperature exists. As V_{sd} increases, the dependence of that gap approaches that shown by curve C, and in the strong interband coupling limit (V_{sd} large compared to V_{ss} and V_{dd}) the smaller gap takes on the characteristics of the larger gap, shown by curve A.

Even in the strong interband coupling limit, the SMW theory predicts the existence of two different energy gaps unless $N_s = N_d$, in which case both gaps display BCS temperature dependence and satisfy the BCS relation $2\Delta(0) / kT_c = 3.526$. In general, the SMW model can be regarded as a specific treatment of energy gap anisotropy which may be applicable to superconductors displaying larger amounts of gap anisotropy than are considered in many theories (40,54).

Electron Tunneling

Electron tunneling is a quantum-mechanical effect. Classically, an

electron cannot penetrate into an insulating region; however, if the wave function of the electron extends through this forbidden barrier, there is a finite probability that the particle will be found on the other side. This probability depends upon such factors as the thickness and height of the barrier, the densities of electron states on either side of the barrier, and the applied voltage.

A tunnel junction, as we have seen, consists of two metals separated by a thin oxide layer. The tunneling current as a function of applied bias voltage depends markedly on whether neither, one, or both of the metals is in the superconducting state. We will discuss qualitatively the current-voltage characteristics of the three cases.

Figure 13a shows the case in which both metals are in the normal state. For $T = 0$, the shaded regions of occupied states fill up to the Fermi energy and then cut off sharply. An applied voltage across the junction has the effect of moving one Fermi level relative to the other, and one can see that the number of electrons which can tunnel increases in proportion to the applied voltage; hence, the current should increase linearly with applied voltage as shown in the figure.

Figure 13b shows the case in which one metal is superconducting and the other is in the normal state. At $T = 0$, no current can flow until the applied voltage corresponds to an energy value of Δ_1. If the current is proportional to the density of states, the singularity in the superconducting density of states gives rise to a rapid increase in current with applied voltage, after which the current approaches the same voltage dependence as when both metals are in the normal state. At temperatures

above zero, the thermal excitation of electrons causes a current to flow before the applied voltage reaches a value corresponding to Δ_1, as shown in the figure. The superconducting energy gap is strongly temperature-dependent and the current-voltage characteristics of a tunnel junction containing one or more superconductors vary with temperature.

When both metals of the tunnel junction are in the superconducting state (Figure 13c), no current will flow until the bias voltage reaches a value such that eV equals $(\Delta_1 - \Delta_2)$, at which point the current rises rapidly. As the voltage increases further, the number of electrons available for tunneling remains the same but the density of available states decreases, thereby causing a decrease in the current with applied voltage. At a voltage corresponding to an energy of $(\Delta_1 + \Delta_2)$ the current again rises very rapidly with increasing applied voltage until it assumes a voltage dependence again corresponding to the normal state of both metals. It is seen that the positions of the initial current peak and the subsequent minimum provide a measure of $2\Delta_2$, the magnitude of the smaller of the two energy gaps.

The calculation of the current flowing across a tunnel junction is based on the assumption that the transition of electrons from one side of the barrier to the other can be treated as an ordinary quantum-mechanical barrier penetration problem. Then the transition probability from a state k on one side of the barrier (left) to a state k' on the other side (right) can be written as

$$P_{kk'} = \frac{2\pi}{\hbar} |M|^2 N' (1 - f') \quad , \qquad (3\text{-}13)$$

where N' is the density of states on the right side and f' is the Fermi function giving the probability that the state k' is occupied. One can determine the current from left to right by summing over the occupied states on the left and multiplying by the electronic charge. When a voltage V is applied to the junction, the resultant tunneling current will be the sum of the two one-way currents. Therefore we can write the current as

$$i(V) = Ae \int_{-\infty}^{+\infty} \{ N_1(E)\, f(E)\, N_2(E - eV)[1 - f(E - eV)] - [N_1(E)\, f(E - eV)\, N_2(E - eV)\, (1 - f(E))] \}\, dE \quad , \quad (3\text{-}14)$$

where we take E as the energy measured from the Fermi level. We can collect terms to obtain

$$i(V) = Ae \int_{-\infty}^{+\infty} N_1(E)\, N_2(E - eV)\, [\, f(E) - f(E - eV)\,]\, dE \, . \quad (3\text{-}15)$$

This is the general expression for the current flowing through a tunnel junction as a function of applied bias voltage.

To obtain the current in a normal-superconducting junction such as was measured in this experiment, $N_1(E)$ is replaced by the superconducting density of states given by Equations (3-10) and (3-11). At $T = 0$ all the contribution to the tunneling current will come within the energy region $E = 0$ to $E = eV$, so for $T = 0$ we have, after evaluating the integral in (3-15) above,

$$i(V) = Ae\, N_1(0)\, N_2(0)\, \{ (eV)^2 - \Delta^2 \}^{\frac{1}{2}} \, . \quad (3\text{-}16)$$

From this we can obtain the normal-superconducting differential

conductance

$$(di/dv)_{ns} = Ae^2 N_1(0) N_2(0) \frac{(eV)}{[(eV)^2 - \Delta^2]^{\frac{1}{2}}} , \qquad (3\text{-}17)$$

and the normalized conductance is given by

$$\sigma = \frac{(di/dv)_{ns}}{(di/dv)_{nn}} = \frac{(eV)}{[(eV)^2 - \Delta^2]^{\frac{1}{2}}} . \qquad (3\text{-}18)$$

Thus we see that at $T = 0$ the normalized conductance is exactly equal to the superconducting density of states.

For temperatures above zero the Fermi functions are no longer sharp and the equivalence of the density of states and the normalized conductance no longer exists. In that case one is forced to revert to the integral in Equation (3-15), which can be differentiated to obtain an expression for the conductance of a tunnel junction. Bermon (70) writes Equation (3-15) in a slightly different form (for the case of a normal-superconducting junction)

$$i(V)_{ns} = \frac{C_N}{e} \int_{-\infty}^{+\infty} \rho_s(E) [f(E - eV) + f(E)] dE , \qquad (3\text{-}19)$$

where C_N is the conductance with both metals in the normal state, and $\rho_s(E)$ is the reduced superconducting density of states (Equation (3-12)). This can be differentiated with respect to the bias voltage to obtain

$$(di/dv)_{ns} = C_N \int_{-\infty}^{+\infty} \rho_s(E) \frac{1}{kT} \left[\frac{\exp\left(\frac{E-eV}{kT}\right)}{\left\{\exp\left(\frac{E-eV}{kT}\right) + 1\right\}^2} \right] dE . \qquad (3\text{-}20)$$

This expression gives the normalized differential conductance for an n-s tunnel junction containing a BCS model superconductor. In the following chapter when it is stated that we calculated the BCS conductance following Bermon, that calculation will be the numerical evaluation of the above integral using the computer program which Bermon has included in his manuscript.

RESULTS AND DISCUSSION

Introduction

The electron tunneling data for a given tunnel junction consist of a number (approximately 10) of single temperature X-Y recorder traces of the tunneling conductance, di/dv, as a function of applied dc bias voltage. A di/dv trace always was taken with the sample in the normal state and the data analysis was done in terms of the normalized tunneling conductance, given by

$$\sigma = \frac{(di/dv)_{ns}}{(di/dv)_{nn}} \quad . \tag{4-1}$$

The following discussion is based on the data obtained on nine tunnel junctions.

As the temperature of an n-s junction is lowered the normalized conductance within the energy gap region decreases, and at $T = 0$ the conductance of the junction should equal zero for bias voltages such that $|eV| < \Delta$, where Δ is the energy gap parameter. An extrapolation to $T = 0$ of the σ_o vs t curve, where σ_o is the normalized conductance at zero bias voltage and t is the reduced temperature T/T_c, did not reach zero conductance for most of our junctions. Therefore, the contribution to di/dv from a parallel conductance mechanism was subtracted from the data before the analysis was attempted. Unless otherwise specified, all data reported in the following will have been normalized and corrected for the presence of parallel conductance. The uncorrected data are available

upon request.

The analysis of the data must rely most heavily on the normalized conductance curves themselves. In addition, however, we have plotted σ_o as a function of reduced temperature. This minimum value of the normalized conductance curve should be related to the value of the energy gap parameter, and in fact Bermon (70) has calculated numerically this relationship for a superconductor with a BCS density of states opposite a normal metal.

The crystallographic structure of the tunnel junctions was determined by examination of standard Laue X-ray diffraction patterns. These data indicate that the degree to which the bulk sample (thorium) is single crystal in nature has a striking effect on the conductance curves which one obtains.

The most acceptable fit to the data has been obtained in terms of the Suhl, Matthias, and Walker (15) model of a two-band superconductor. The results are not decisive, and the conclusions reached will be suggestive only. Nevertheless, we will attempt to show how our results indicate the presence of two-gap behavior in single crystal thorium and single-gap behavior in polycrystalline samples. We also will discuss our results in view of other experimental results on thorium.

Results

The tunnel junctions can be categorized by inspection of their Laue patterns into three groups: 1) those for which the thorium in the junction area was single crystal, 2) those for which the thorium pattern displayed a single crystal pattern superimposed on a polycrystalline background, and 3) those for which the thorium sample was fully polycrystalline. The

X-ray diffraction results are given in Table 3, along with the transition temperatures of the junctions. It is seen that four of the nine tunnel junctions contained single crystal thorium; these are Au on Th Nos. 5 and 6, and Ag on Th Nos. 1 and 2. Junction Au on Th No. 9 was strictly polycrystalline, while the remaining junctions involved thorium which was partly single crystal and partly polycrystalline, with the exception of Au on Th No. 4, for which no Laue pattern was obtained.

Table 3. X-ray diffraction results and transition temperatures for the tunnel junctions

Junction	Orientation	Crystalline state	T_c(K)
Au on Th No. 1		Mixed[a]	1.316
Au on Th No. 4			1.387
Au on Th No. 5	[110][b]	Single	1.394
Au on Th No. 6	[110][b]	Single	1.385
Au on Th No. 7		Mixed[a]	1.362
Au on Th No. 8		Mixed[a]	1.332
Au on Th No. 9		Poly	1.39
Ag on Th No. 1	Off axis[c]	Single	1.375
Ag on Th No. 2	[100][b]	Single	1.335

[a]Partially single crystal

[b]Within 10° of the axis

[c]Approximately 20° from [100], [110], and [111] axes

The plots of σ_o vs t for the tunnel junctions appear in Figures 14-16. The solid curve in each case is that calculated using Equation (3-20) and a BCS temperature dependence for the energy gap as tabulated by Muhlschlegel (71). One can see from Figure 14 that the conductance minima of the four single crystal sample tunnel junctions display a common temperature dependence. Figure 16 shows that three of the junctions exhibit a temperature dependence which is very similar to the solid BCS curve; these junctions are the ones for the polycrystalline sample (Au on Th No. 9), the sample for which we have no Laue pattern (Au on Th No. 4), and one of the partly single crystal samples (Au on Th No. 1). In the following, as a matter of convenience, we shall refer to these junctions as BCS-like. The remaining two junctions, both of which exhibited a mixed X-ray pattern, show a dependence (Figure 15) which is intermediate between the curve for the single crystal samples and the solid BCS curve.

The tunnel junctions which will be discussed in detail are three which exhibit the three types of behavior displayed in Figures 14-16. The three sets of normalized conductance curves for those junctions, one set for each of these types of behavior, are shown in Figures 17-19. When referring to these and similar curves, we will call the region between the symmetric maximum points the gap region, and we will label the regions of the maxima the shoulders of the di/dv trace. Although there are differences in shape in the shoulder regions for tunnel junctions of a given type, they all do exhibit the same σ_o vs t dependence and all lowest temperature traces fall very close to the same curve in the gap region. Furthermore, general characteristics of a given junction, such as relative

shoulder height and trace width, do not vary irregularly over the temperature range measured. For these reasons the normalized conductance curves of only one junction within each type were analyzed in detail, since these curves were taken as representative of all the tunnel junctions within that type. The traces for Au on Th No. 6 in Figure 17 correspond to the single crystal junctions listed in Figure 14; the Au on Th No. 7 curves in Figure 18 are representative of the partly single crystal junctions of Figure 15; and the curves for Au on Th No. 4 shown in Figure 19 are taken as representative of the BCS-like junctions (Figure 16).

Discussion

Several thin film tunnel junctions were measured to establish our ability to evaporate thin films successfully, and to verify the proper operation of the electronic detection system. The value of the reduced energy gap parameter of aluminum as obtained from an Al-Al_2O_3-Pb junction is shown in Figure 20. The value of the gap parameter was determined from the sum and difference peaks of the Pb and Al gap contributions as previously discussed (page 41). These results predict a zero temperature energy gap value of $2\Delta = 0.344$ meV and are in good general agreement with the results of Douglass and Meservey (72). An Al-Al_2O_3-Al junction gave a zero temperature estimate of the aluminum energy gap of 0.350 meV, which is in good agreement with our previous result.

The calibration procedure used for the tunneling bridge appears to be valid, since both of the above junctions showed the expected value of zero conductance at lowest temperatures. The linearity of the bridge had been checked previously, so the above results established the satisfactory

operation of the electronics. Specifically, this showed that the parallel conductance which was observed in the case of the thorium tunnel junctions was not due to spurious electrical measurements.

The origin of the parallel conductance which was subtracted from the thorium data is not known. The strongest evidence (in this experiment) that the effect is indeed an independent mechanism in parallel with the tunnel junction is that the corrected data show consistent behavior. The following relation was used to correct the data to obtain the normalized conductance of a tunnel junction:

$$\sigma = \frac{(di/dv)_{ns} - (di/dv)_{\shortparallel}}{(di/dv)_{nn} - (di/dv)_{\shortparallel}} , \qquad (4\text{-}2)$$

where $(di/dv)_{\shortparallel}$ is the estimated parallel conductance contribution. The value of $(di/dv)_{\shortparallel}$ for each junction is given in Table 4. It is seen from the table that the value of the correction was different for each junction, and yet the corrected results for each type of junction lie close to a single σ_o vs t curve. Figure 21 is a comparison of normalized conductance curves before and after the parallel conductance correction was made, and one can see that the essential shape of the conductance curve remains unchanged, thus indicating that the physical information is not removed from the curve by the correction.

The existence of metallic shorts through the junction oxide often is suggested as a cause for the excess conductance of tunnel junctions. Marcus (44) and Rowell and Feldmann (73) have presented evidence for the existence of such metallic shorts in superconductor-superconductor tunnel

junctions, and while their arguments are related to superconducting bridges, the possibility of normal metal bridges (gold in our case) in tunnel junctions is just as strong. A number of attempts at junction fabrication were made using metals other than gold or silver for the cross-evaporated film. We tried aluminum, tin, indium, and lead, and in all

Table 4. Parallel conductance corrections for the tunnel junctions

Junction	$(di/dv)_{\parallel}$
Au on Th No. 1	approx 0.15
Au on Th No. 4	0.190
Au on Th No. 5	0.0
Au on Th No. 6	0.099
Au on Th No. 7	0.311
Au on Th No. 8	0.659
Au on Th No. 9	0.148
Ag on Th No. 1	0.168
Ag on Th No. 2	0.832

cases the resistances of the junctions never fell below 10 kΩ. This suggests that the gold and silver (heavier atoms with higher energies associated with a higher melting point) may penetrate part way into the oxide. Such penetration would reduce the effective oxide thickness, thus increasing the probability of tunneling, but it could also lead to metallic shorts through the oxide.

Zeller and Giaever (74) have embedded small tin spheres in tunnel

junction oxides. Their data on such junctions showed a normal state resistance peak (or conductance minimum) at zero bias which increased when the tiny spheres went superconducting. The junctions in our experiment showed no such normal state effect and inasmuch as we are concerned with mechanisms which could increase the conductance rather than decrease it, the possibility of superconducting thorium bridges through the thorium oxide was ruled out.

Irrespective of the cause, excess tunneling conductance has been documented by other experimenters. While Shen (39) does not report on the magnitude of the effect in his experiments, MacVicar and Rose (35) state a criterion for rejecting tunnel junctions which show, in their opinion, too much "excess current". We have estimated from the published data on one of their best junctions that the amount of parallel conductance present in that junction was approximately 0.10, of the same magnitude as the corrections made in this experiment.

The parallel conductance correction was chosen to be that value of $(di/dv)_{11}$ in Equation (4-2) which caused the σ_o vs t curves to extrapolate to zero at $t = 0$. Since the experimental temperatures did not extend much below 0.3 K, there was room for some error in the extrapolation, and this is the major uncertainty associated with the conductance values. One can estimate the size of the conductance uncertainty associated with the parallel conductance correction by examining Equation (4-2). The quantity $(di/dv)_{nn}$ is always very close to 1.00. The possible error in the conductance values is least when $(di/dv)_{ns}$ is large and $(di/dv)_{11}$ is small; the possible error is greatest when $(di/dv)_{ns}$ is small and $(di/dv)_{11}$ is

large. Therefore the uncertainty due to the conductance corrections will be largest at lower temperatures and for junctions having the largest corrections; the uncertainty will be smallest at higher temperatures and for the junctions with the least parallel conductance corrections. The error bars shown in Figures 14 and 15 represent typical estimated uncertainties for a parallel conductance correction of 0.20.

A theoretical fit to the data must reproduce both the σ_o vs t and the normalized conductance curves in their entirety at all temperatures. The approach taken was first to find calculated curves which could fit the σ_o vs t graphs and second to use the fit parameters in the calculation of conductance curves over the range of experimental dc bias. The curves of Figures 14 and 15 could not be fitted using a single energy gap with BCS temperature dependence. Therefore, the SMW notion of two energy gaps was adopted as a guide.

The initial work was done with the conductance minimum curve for the single crystal junctions (Figure 14). As a first step, two different energy gaps with BCS reduced temperature dependence and a common T_c were used. This common transition temperature was assumed since the $V_{sd} = 0$ limit (giving two different transition temperatures as shown in Figure 1) seemed physically unreasonable. All of the attempts failed to yield a good fit to the conductance minimum curve for these single crystal junctions. Although the mixture of the two energy gaps as described does deviate from the single-gap BCS curve in the direction of the experimental results, it was not possible to achieve sufficient curvature by this method to match the experimental conductance minimum curve.

Next, a fit to the data was attempted using two energy gaps with two transition temperatures, both of which had BCS temperature dependence. The shapes of the σ_o vs t curves were reproduced much better using this approach, and the closest fit was obtained for energy gap parameter values of 0.190 and 0.090 meV, and for an equal contribution from each gap. However, this calculated σ_o vs t curve showed too much curvature in the region of the transition temperature for the smaller gap. The two-band theories (15,29) suggest that the larger gap does not change markedly with increasing V_{sd} for pure samples (15) or with increasing impurity concentration for impure samples (29). Hence, as a final approximation, we assumed the larger gap to have $\Delta(0) = 0.190$ meV and a BCS temperature dependence, and then determined values of the smaller gap parameter which gave a close fit to the σ_o vs t curves. These gap parameter values are shown in Figure 22 where the curves for the two energy gaps are suggestive of curves A and A' in Figure 1.

The next step was to calculate the differential conductance curves corresponding to these values of the energy gap parameters, and this was done using a modified version of Bermon's (70) computer program which calculates differential conductance curves based on the BCS density of states. As was mentioned previously, the normalized conductance traces are very similar for all single crystal samples and were calculated only for the experimental temperatures of junction Au on Th No. 6. The fits at four representative temperatures shown in Figure 23 are quite good within the energy gap region but show some deviation in the region of the shoulders (the deviation in the shoulder region will be discussed in more detail

later). The striking fact is that the fits are of nearly the same accuracy at all temperatures.

Figure 22 indicates that the second energy gap goes to zero at a transition temperature near 1.0 K, while it is more reasonable physically for the second gap to have a high temperature tail extending to $t = 1$ as is shown by curve B in Figure 1. If the second gap followed this type of curve (indicated by the solid circles in Figure 22) instead of going to zero, the change in the calculated conductance curves for those temperatures would be approximately 1 to 2%. Since a change of this magnitude is within the estimated uncertainties, it is impossible to state definitely whether or not a second transition temperature should be present with the second gap.

The gap mixing ratio of 1 : 1 was retained and a similar fitting procedure was attempted on the conductance minimum curve of the partly single crystal junctions shown in Figure 15. The conductance minimum curve for these junctions was fitted using energy gaps shown in Figure 24, with the calculated conductance minimum curve shown by the dashed line in Figure 15. Again we imposed a BCS reduced temperature dependence on the larger gap and the temperature dependence of the smaller gap was dictated by the best fit. The entire differential conductance curves then were calculated and the quality of the fits to junction Au on Th No. 7 was similar to that obtained for the single crystal junctions. The fits at four temperatures are shown in Figure 25. The energy gaps shown in Figure 24 resemble the moderate interband coupling curves C and A of Figure 1.

The conductance minimum plot for three of the tunnel junctions was

BCS-like as is shown in Figure 16. Junction Au on Th No. 4 was chosen as a representative junction of this group, and the energy gap parameter values which produce the conductance minimum values for the junction are shown in Figure 26. The single-gap conductance curves calculated from these energy gaps are shown in Figure 27 for some representative temperatures. The junctions of this type were polycrystalline, or nearly so, and the results resemble the case of a single energy gap in the strong interband coupling limit discussed by SMW (curve A in Figure 1).

The analyses which have provided the best fits to the tunneling data have shown a surprising correspondence to the predictions of SMW for different values of V_{sd} in a pure superconductor. In addition, a correlation appears to exist between the crystalline state of the bulk sample and the three types of observed tunneling characteristics, although an explanation for this correlation is not immediately evident.

The analysis in terms of two energy gaps which suggest two different transition temperatures is appropriate only for those junctions in which the thorium was completely single crystal in the junction region. The energy gaps obtained are similar to those for the case of V_{sd} being zero or very small in the SMW theory; also, unless the two gaps have these different temperatures dependences a reasonable calculated fit to the data cannot be obtained.

One partly and one wholly polycrystalline sample are well described in terms of one energy gap which has a BCS temperature dependence. This case of a single energy gap appears to correspond to the strong interband coupling limit with $N_s = N_d$ in the SMW theory. It equally as well could be the

result of impurity or grain boundary scattering having removed the anisotropy that obviously exists in the case of the single crystal data.

The temperature dependence of the smaller gap used to fit the partly single crystal junction data is close to that of curve C which is sketched in in Figure 1 as the moderate interband coupling case, but this is probably coincidental. The energy gap dependence in the moderate interband coupling case should lie between curves B and A in the figure, and the position of curve C is only one of a large number of possibilities. If polycrystallinity introduced scattering, one would expect the smaller energy gap to increase and the larger gap to decrease towards a common limiting value (75). The smaller gap does not increase with polycrystalline structure, and the larger gap does increase, so that an analysis in terms of impurity effects seems inadequate for these partly single crystal samples.

In the SMW theory V_{sd} is a microscopic quantity which is related to the local coupling between s and d electrons, and one does not expect it to be changed significantly by the presence of grain boundaries. Furthermore, the SMW theory considers only the case of pure samples, and it is not reasonable to assume that an increase in scattering could lead to an increase in the coupling energy between s and d electrons. The resemblance of our results to the SMW theory for the moderate and strong interband coupling cases should be considered fortuitous.

On the other hand, an explanation of our results in terms of grain boundary scattering of the electrons, while it could account for single energy gap behavior in the polycrystalline case, seems unable to explain

the case of the partly single crystal tunnel junctions. We cannot suggest other explanations and are forced to present our results without an accompanying satisfactory explanation for them.

The correlation between crystalline structure and the three types of tunneling behavior observed is complete with the exception of one partly single crystal junction which shows BCS-like characteristics. The X-rays with which the Laue patterns were obtained penetrate much deeper into the sample than do the tunneling electrons (a complete discussion of X-ray diffraction has been given by Cullity (76)), and one can argue (though not strongly) that polycrystalline regions in a sample tend to predominate near the surface (77), so that in this case it would be possible for tunneling electrons to see a strictly polycrystalline sample while the deeper penetration of the X-rays allows them to see both single and polycrystalline regions. This could be a possible explanation for the BCS-like tunneling behavior of one of the partly single crystal junctions.

The penetration into the bulk sample by the tunneling electrons is much less for the transition elements than for many other metals (43), and this is the reason why surface purity is critical to the preparation of good tunnel junctions on these elements. This fact also serves to reemphasize the difficulties in obtaining trouble-free tunneling data on the transition metals.

There are a number of difficulties associated with the analysis of the data. One must consider the deviation of the data from the calculated conductance curves in the shoulder regions (see Figures 23, 25, and 27). Deviations from BCS predictions in the shoulder regions are common in

tunneling measurements, even in the case of simpler metals than the transition elements. Such deviations were seen in the early measurements by Giaever, Hart, and Megerle (11), who postulated that the effect was due to a smearing of the energy gap. It would not be surprising that effects other than thermal smearing could influence the singularity in the density of states at the gap edge. Anisotropy in the energy gap might produce a broadening of the shoulders. A slightly energy-dependent gap parameter could produce such deviations also, but the effect must be regarded as not fully explained.

The reason for analyzing the data primarily in terms of the minimum point on the conductance curves is related to this shoulder problem. For the case of two energy gaps, both of which contribute to the conductance, it is very difficult to estimate the contribution to the conductance of the separate energy gaps unless one has a detailed picture of the normalized conductance associated with each gap. On the other hand, the minimum point of the conductance curve is well-defined and can be related easily to values of the energy gaps via Bermon's calculations. The minimum of the conductance curve is therefore the most convenient parameter to use as a stepping-stone towards the calculation of entire conductance curves.

The equal weighting of the two gaps in our data analysis was arrived at after a large number of attempts in which parameters such as energy gap magnitude, transition temperature, and relative contribution of the s and d bands were varied over a large range. The best fit to the conductance curves and the conductance minimum curves dictated a relative contribution of 0.502 for the d band and 0.498 for the s band (this does not imply

equality of the thermodynamic densities of states, N_s and N_d). This result was assumed to remain unchanged for both of the two-gap analyses. The experimental evidence for two energy gaps in niobium, which has an outer electronic configuration of $4d^4\ 5s^1$, indicates that $N_s << N_d$. The outer electronic configuration of thorium is $6d^2\ 7s^2$, and in view of this fact, one might expect thorium to have a larger value of N_s / N_d than is suggested for niobium. It also is possible that tunneling selection processes result in a much higher value of N_s than would be observed in measurements of thermodynamic variables.

The results of this experiment suggest that if the SMW two energy gap theory is applicable to thorium, it applies only to single crystal samples. Experiments on other transition metals which indicate the presence of a second gap have been done on single crystal samples almost without exception. This is true of the thermal conductivity data on niobium due to Carlson and Satterthwaite (27), the specific heat measurements on niobium, tantalum, and vanadium by Shen, Senozan, and Phillips (23), and the electron tunneling measurements on niobium by Hafstrom and MacVicar (37). The only exception to the single crystal criterion is the specific heat data of Shen et al. on a polycrystalline niobium sample; these data did indicate the presence of a second gap, although the effect was not as pronounced as in the case of the single crystal sample.

Unfortunately, since all previous experimental data on thorium have been obtained using polycrystalline samples, no direct confirmation of our results is possible. The normal state resistivity data of Peterson et al. (49) do suggest that thorium is a two-band metal. Their low temperature

data display a $T^{3.5}$ temperature dependence, which is close to the T^3 dependence predicted for the resistivity of an s-d band metal. This $T^{3.5}$ dependence is not evident in the published paper (49) because of the large temperature range over which the data were plotted, so a low temperature plot of the data is shown in Figure 28 to illustrate it. This result generally supports our two-band analysis of thorium.

Anderson, Peterson, and Finnemore (53) have measured the anisotropy in polycrystalline rods of thorium. An expression for the anisotropy constant $\langle a^2 \rangle$ is given by the relation

$$\langle a^2 \rangle = \frac{\langle (\Delta_p - \langle \Delta_p \rangle_{av})^2 \rangle_{av}}{\langle \Delta_p \rangle_{av}^2} , \qquad (4\text{-}3)$$

where Δ_p is the value of the energy gap at a point on the Fermi surface. Our data suggest energy gap parameter values of 0.190 meV and 0.090 meV, and a variation in Δ of this magnitude gives a value of $\langle a^2 \rangle = 0.127$, when the s and d parts of the Fermi surface are weighted equally (this may not be a reasonable assumption). A value of $\langle a^2 \rangle = 0.021$ was obtained by Anderson et al., however this result was obtained by using the theory of Markowitz and Kadanoff (54), which was not designed to treat large amounts of anisotropy. The Anderson et al. value may be an underestimate and the correct value may lie between the two values of $\langle a^2 \rangle$ suggested above.

It is difficult to draw conclusions from the thermal conductivity data for thorium obtained by Cappelletti and Finnemore (51). The BCS theory was extended by Bardeen, Rickayzen, and Tewordt (BRT) (55) to a treatment of thermal conductivity, and the thorium data do not follow the

BRT curve. The data lie close to the BRT curve (for a superconductor with a transition temperature of 1.36 K) near T_c, but lie above it for all temperatures below 0.9 T_c. This sort of behavior is to be expected for a superconductor with an anisotropic energy gap, since the contributions due to a smaller gap tend to dominate at low temperatures. The samples used by Cappelletti and Finnemore were definitely polycrystalline, so we do not expect anisotropy effects as large as those observed for our single crystal samples.

Critical field data on thorium due to Decker and Finnemore (52) lie within 0.3% of the BCS prediction on a standard plot of the deviation from a fiducial parabola. These data were obtained from two samples with resistivity ratios of 1200 and 35. The results for the two samples were very nearly identical and only those for the purer sample are reported in the literature. We examined the sample with the lower resistivity ratio under a microscope and found the grain sizes to be approximately 0.02 mm. In addition, the high resistivity ratio sample, which was 3 mm in diam by 25 mm long, should have contained crystallites with dimensions no larger than 1 to 2 mm (77). In view of the fact that the grain sizes in the high resistivity ratio sample could be close to the same size as the area of our tunnel junctions, one might expect some degree of two-gap behavior. In fact, a calculation of the electronic specific heat using the observed critical field curves does show a suggestion of an extra contribution to the specific heat around T = 1 K, which is the same temperature as the apparent transition temperature of the second gap in part of our data analysis.

Clem (75) has calculated the critical field curve for a superconductor having two energy gaps and two transition temperatures appropriate to our single crystal samples ($T_s \sim 0.5\ T_d$ and $\Delta_s \sim 0.5\ \Delta_d$) and $N_s = N_d$. This calculation may be appropriate to a superconductor for which our analysis (of the single crystal junctions) is valid. In the calculation, the maximum deviation from the BCS single gap prediction comes at a reduced temperature of approximately 0.5 and should be about 5% (a very large effect). This was not observed for Decker and Finnemore's samples, and this suggests that N_s is not equal to N_d for thorium. Specific heat data on single crystal thorium would help to answer a number of the questions which our work has introduced.

CONCLUDING REMARKS

The results of this experiment strongly suggest that thorium does not have an isotropic energy gap. It has been shown that other experimental data on thorium are consistent with a two-band electronic structure, similar to the transition metals. The present data have been analyzed in terms of a two-band model of a superconductor, and in fact the SMW theory seems appropriate for thorium single crystals.

We have found a correlation between apparent two energy gap behavior and the crystalline structure of the sample. Single crystal samples seem to show a strong two-gap effect, while polycrystalline samples display single energy gap BCS-like characteristics. This correlation implies that future electron tunneling measurements should be performed on single crystal samples, and since our results were obtained on bulk thorium samples, the same suggestion appears to be in order for some bulk sample thermodynamic measurements, such as the specific heat.

We have not been able to offer a conclusive explanation for our results. However, we feel that the results do warrant further attempts to observe the two-gap nature of thorium.

ACKNOWLEDGEMENTS

First, I want to thank my wife, Sue, for the encouragement and understanding which she continually offered during our years of graduate school. The contributions which she has made have not been without sacrifice, and they are deeply appreciated.

Dr. Werden Keeler has contributed heavily to this work. His assistance, his advice, and the many discussions with him have been invaluable. In addition, I wish to thank him for the use of the tunneling bridge which he constructed.

I wish to thank Dr. D. K. Finnemore, my major professor, for his help and suggestions during the course of this work, and especially for his communications from England during the time that this thesis was being written. The members of Dr. Finnemore's group have also contributed helpful discussions during the course of this work.

I appreciate the time and help that Dr. C. A. Swenson has afforded me in his role as substitute major professor.

Finally, I would like to acknowledge John R. Hopkins.

BIBLIOGRAPHY

1. J. Bardeen, L. N. Cooper, and J. R. Schrieffer, Phys. Rev. 108, 1175 (1957).

2. M. A. Biondi, A. T. Forrester, M. P. Garfunkel, and C. B. Satterthwaite, Rev. Mod. Phys. 30, 1109 (1958).

3. P. L. Richards and M. Tinkham, Phys. Rev. Letters 1, 318 (1958); Phys. Rev. 119, 575 (1960).

4. J. Frenkel, Phys. Rev. 30, 1604 (1930).

5. I. Giaever, Phys. Rev. Letters 5, 464 (1960).

6. J. C. Fisher and I. Giaever, J. Appl. Phys. 32, 172 (1961).

7. I. Giaever and K. Megerle, Phys. Rev. 122, 1101 (1961).

8. J. Bardeen, Phys. Rev. Letters 6, 57 (1961).

9. M. Cohen, L. M. Falicov, and J. C. Phillips, Phys. Rev. Letters 8, 316 (1961).

10. J. R. Clem, On the Relations between the Effective Tunneling Density of States and the Differential Conductance, 1963 (unpublished).

11. I. Giaever, H. R. Hart, Jr., and K. Megerle, Phys. Rev. 126, 941 (1962).

12. J. Nicol, S. Shapiro, and P. H. Smith, Phys. Rev. Letters 5, 461 (1960).

13. D. M. Ginsberg, P. L. Richards, and M. Tinkham, Phys. Rev. Letters 3, 337 (1959).

14. L. N. Cooper, Phys. Rev. Letters 3, 17 (1959).

15. H. Suhl, B. T. Matthias, and L. R. Walker, Phys. Rev. Letters 3, 552 (1959).

16. J. W. Garland, Jr., Phys. Rev. Letters 11, 111 (1963).

17. P. W. Anderson, J. Phys. Chem. Solids 11, 26 (1959).

18. H. M. Rosenberg, Low Temperature Solid State Physics (Oxford University Press, London, 1965), p. 97.

19. A. H. Wilson, Proc. Roy. Soc. (London) A167, 580 (1938).

20. G. W. Webb, Phys. Rev. 181, 1127 (1969).

21. T. H. Geballe, B. T. Matthias, G. W. Hull, Jr., and E. Corenzwit, Phys. Rev. Letters 6, 275 (1961).

22. J. Peretti, Phys. Letters 2, 275 (1962).

23. L. Y. L. Shen, N. M. Senozan, and E. Phillips, Phys. Rev. Letters 14, 1025 (1965).

24. C. C. Sung and L. Y. L. Shen, Phys. Letters 19, 101 (1965).

25. V. Radhakrishnan, Phys. Stat. Sol. 20, 783 (1967).

26. V. Radhakrishnan, Nuovo Cimento 48B, 111 (1967).

27. J. R. Carlson and C. B. Satterthwaite, Phys. Rev. Letters 24, 461 (1970).

28. I. M. Tang, Phys. Letters 31A, 480 (1970).

29. C. C. Sung and V. K. Wong, J. Phys. Chem. Solids 28, 1933 (1967).

30. N. V. Zavaritskii, Sov. Phys.-JETP 21, 557 (1965).

31. M. L. A. MacVicar and R. M. Rose, Phys. Letters 26A, 510 (1968).

32. I. Giaever, in Proceedings of the Eighth International Conference on Low-Temperature Physics, edited by R. O. Davies (Butterworth, Washington, D.C., 1963), p. 171.

33. P. Townsend and J. Sutton, Phys. Rev. 128, 591 (1962).

34. M. D. Sherrill and H. H. Edwards, Phys. Rev. 6, 460 (1961).

35. M. L. A. MacVicar and R. M. Rose, J. Appl. Phys. 39, 1721 (1968).

36. M. L. A. MacVicar, Phys. Rev. B 2, 97 (1970).

37. J. W. Hafstrom and M. L. A. MacVicar, Phys. Rev. (to be published).

38. L. M. Mattheiss, Phys. Rev. (to be published).

39. L. Y. L. Shen, Phys. Rev. Letters 24, 1104 (1970).

40. J. R. Clem, Annals of Physics 40, 268 (1966).

41. A. J. Bennett, Phys. Rev. 153, 482 (1967).

42. J. E. Dowman, M. L. A. MacVicar, and J. R. Waldram, Phys. Rev. 186, 452 (1969).

43. W. L. McMillan and J. M. Rowell, in Superconductivity, edited by R. D. Parks (Marcel Dekker, Inc., New York, 1969), Vol. 1, p. 581.

44. S. M. Marcus, Phys. Letters 20, 236 (1966).

45. A. F. G. Wyatt, Phys. Rev. Letters 13, 401 (1964).

46. J. Appelbaum, Phys. Rev. Letters 17, 91 (1966).

47. R. P. Gupta and T. L. Loucks, Phys. Rev. Letters 22, 458 (1969).

48. J. E. Gordon, H. Montgomery, R. J. Noer, G. R. Pickett, and R. Tobon, Phys. Rev. 152, 432 (1966).

49. D. T. Peterson, D. F. Page, R. B. Rump, and D. K. Finnemore, Phys. Rev. 153, 701 (1967).

50. D. J. Boyle and A. V. Gold, Phys. Rev. Letters 22, 461 (1969).

51. R. L. Cappelletti and D. K. Finnemore, Phys. Rev. 188, 723 (1969).

52. W. R. Decker and D. K. Finnemore, Phys. Rev. 172, 430 (1968).

53. J. W. Anderson, D. T. Peterson, and D. K. Finnemore, Phys. Rev. 179, 472 (1969).

54. D. Markowitz and L. Kadanoff, Phys. Rev. 131, 563 (1963).

55. J. Bardeen, G. Rickayzen, and L. Tewordt, Phys. Rev. 113, 982 (1959).

56. M. B. Maple, J. G. Huber, and K. S. Kim, Sol. St. Comm. 8, 981 (1970).

57. K. W. Taconis, in Progress in Low Temperature Physics, edited by C. J. Gorter (North-Holland Publishing Co., Amsterdam, 1961), Vol. III.

58. Guy K. White, Experimental Techniques in Low-Temperature Physics (Oxford University Press, London, 1968), 2nd ed., p. 327.

59. C. A. Swenson, Critical Reviews in Solid State Physics 1, 99 (1970).

60. D. K. Finnemore, Ames Laboratory of the United States Atomic Energy Commission Data Book DFK-9, 1968 (unpublished).

61. D. T. Peterson, W. E. Krupp, and F. A. Schmidt, J. Less-Common Metals 7, 288 (1964).

62. T. F. Stromberg, Ph.D. thesis, Iowa State University, 1965 (unpublished).

63. Handbook of Chemistry and Physics, edited by C. D. Hodgman (Chemical Rubber Publishing Co., Cleveland, 1962), 43rd ed., p. 2321.

64. J. S. Rogers, Rev. Sci. Instr. 41, 1184 (1970).

65. J. R. Schrieffer, Superconductivity (W. A. Benjamin, Inc., New York, 1964).

66. P. G. de Gennes, Superconductivity of Metals and Alloys (W. A. Benjamin, Inc., New York, 1966).

67. D. K. Finnemore, A Child's Guide to BCS, 1967 (unpublished).

68. J. Bardeen and D. Pines, Phys. Rev. 99, 1140 (1955).

69. L. N. Cooper, Phys. Rev. 104, 1189 (1956).

70. S. Bermon, National Science Foundation Grant No. NSF-GP1100 Technical Report No. 1, 1964 (unpublished).

71. B. Muhlschlegel, Z. Physik 155, 313 (1959).

72. D. H. Douglass, Jr. and R. Meservey, Phys. Rev. 135, A19 (1964).

73. J. M. Rowell and W. L. Feldmann, Phys. Rev. 172, 393 (1968).

74. H. R. Zeller and I. Giaever, Phys. Rev. 181, 789 (1969).

75. J. R. Clem, Ames, Iowa (Private communication).

76. B. D. Cullity, Elements of X-Ray Diffraction (Addison-Wesley Publishing Co., Inc., Reading, Mass., 1956).

77. D. T. Peterson, Ames, Iowa (Private communication).

FIGURES

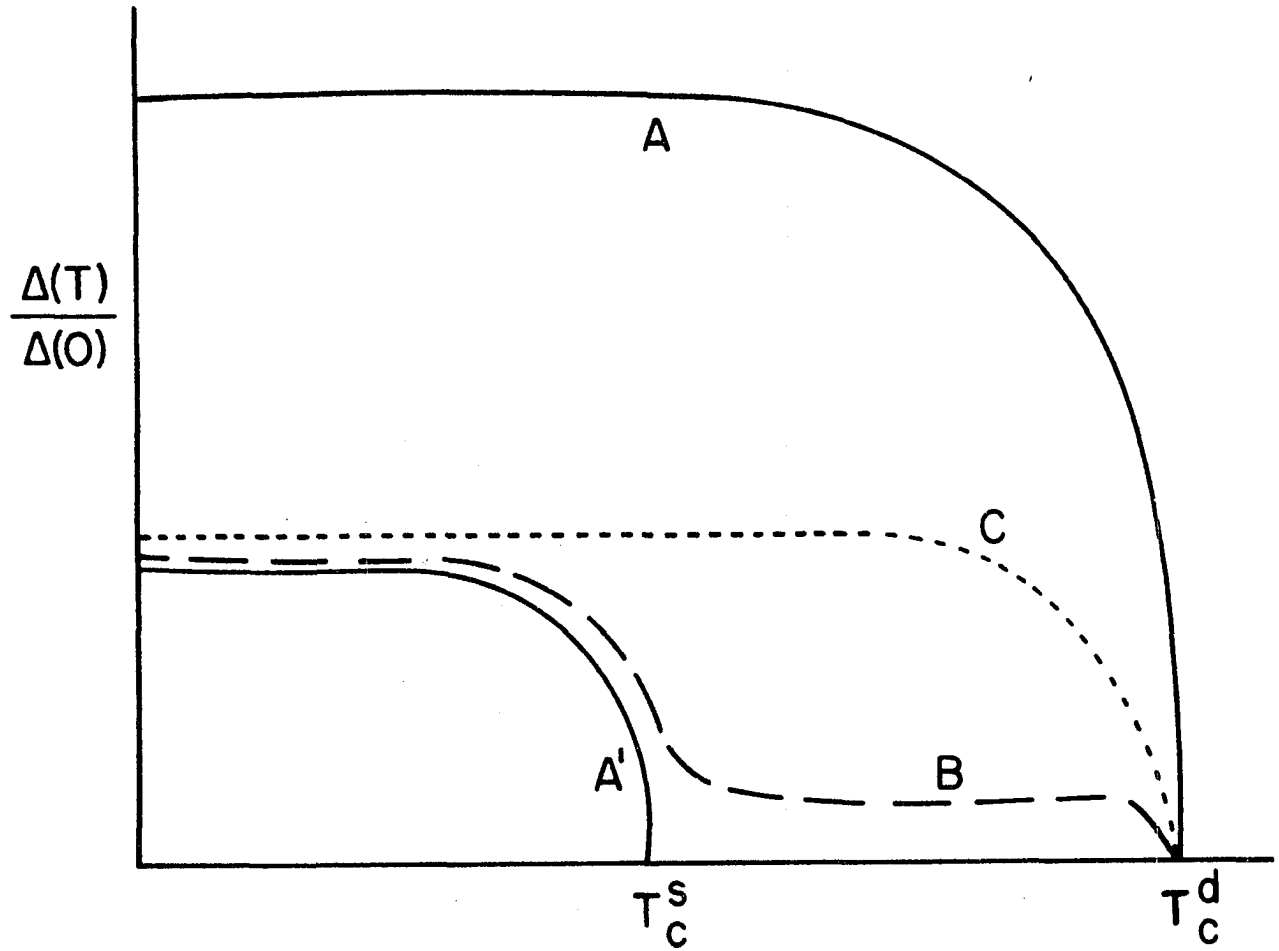

Figure 1. Behavior of the energy gap in a two band superconductor (after SMW). Curve A: BCS dependence of Δ_d; Curve A': Δ_s in the intraband limit ($V_{sd}=0$); Curve B: Δ_s for weak interband coupling; Curve C: Δ_s for moderately strong interband coupling

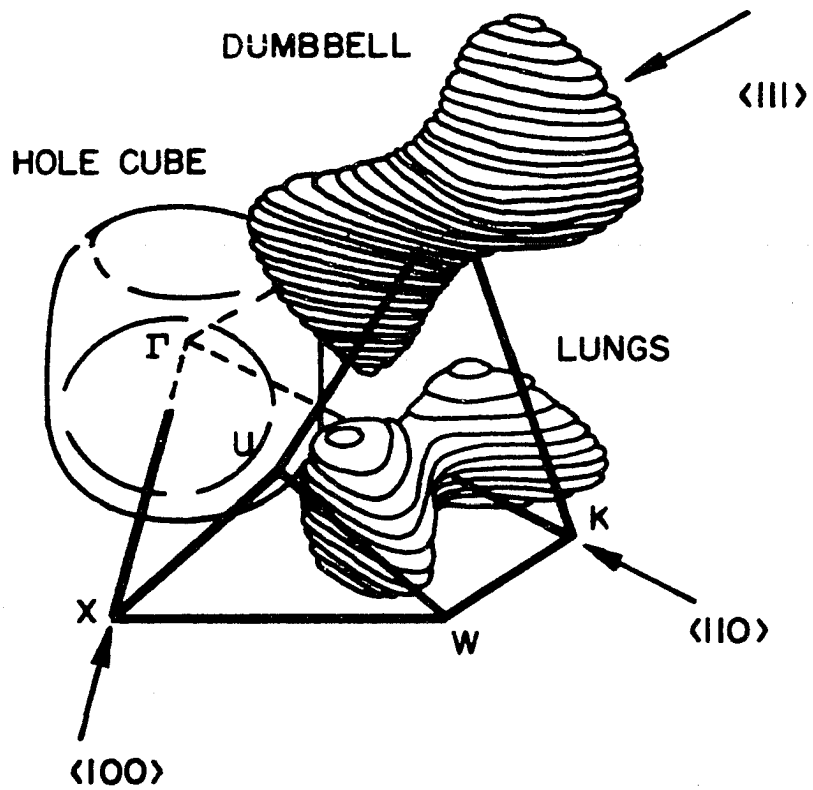

Figure 2. Fermi surface of thorium

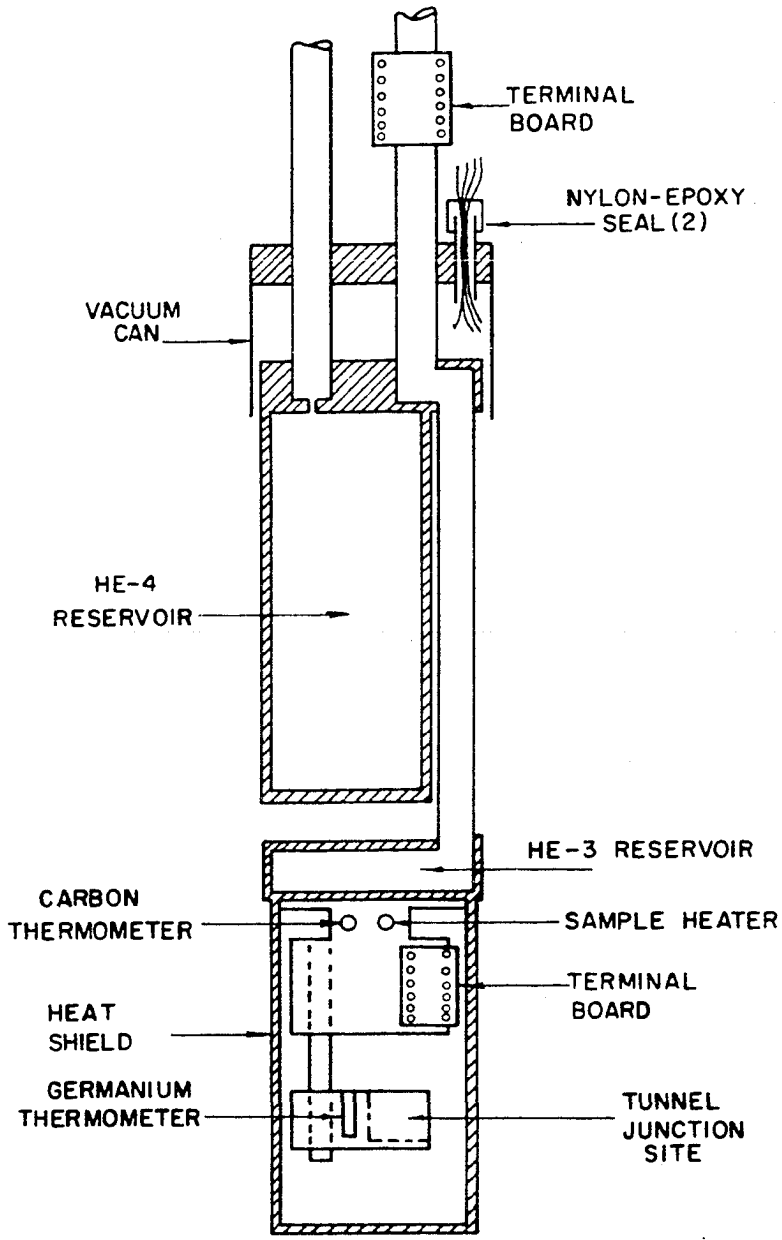

Figure 3. Electron tunneling cryostat

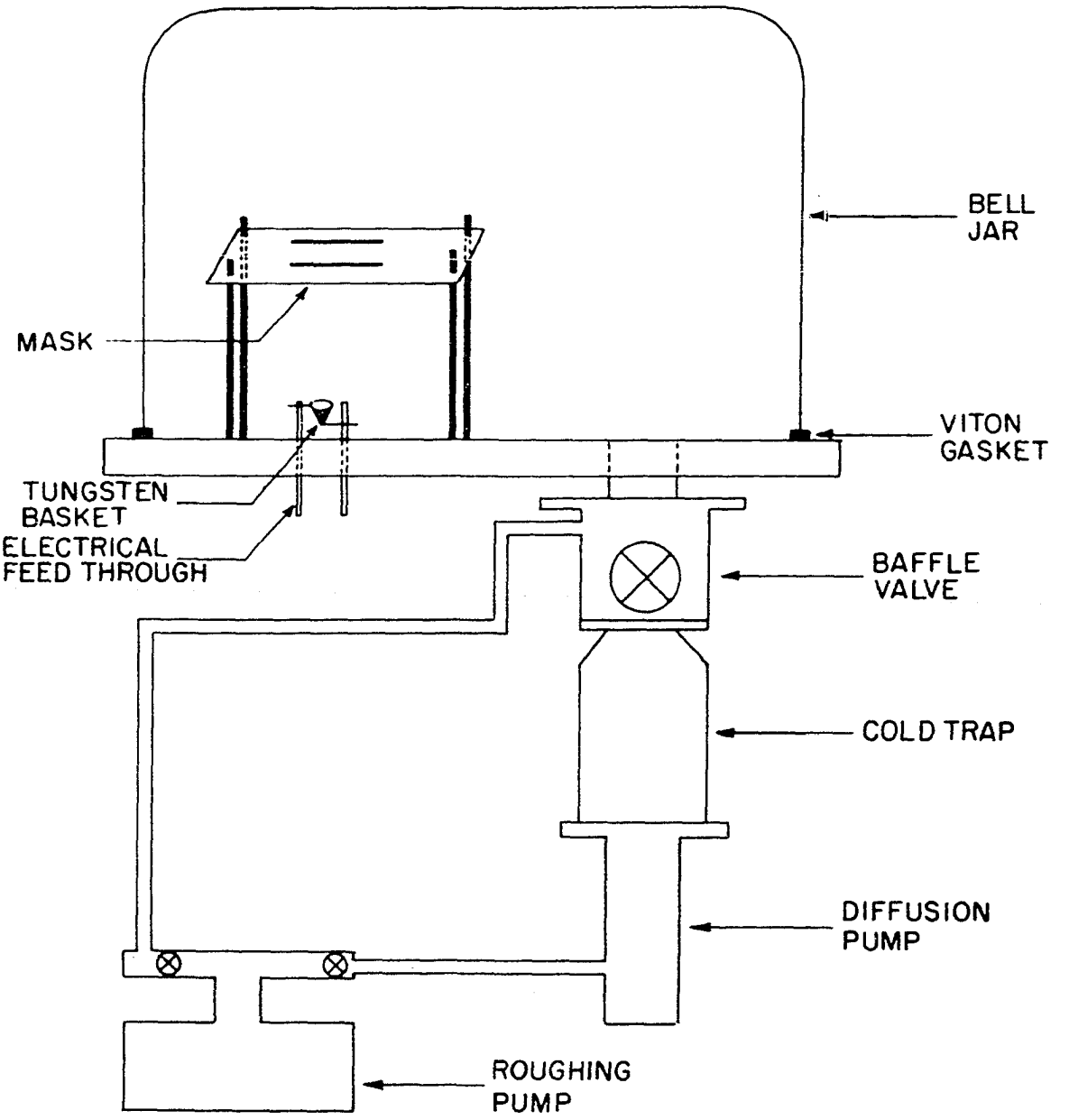

Figure 4. Bell jar evaporation system

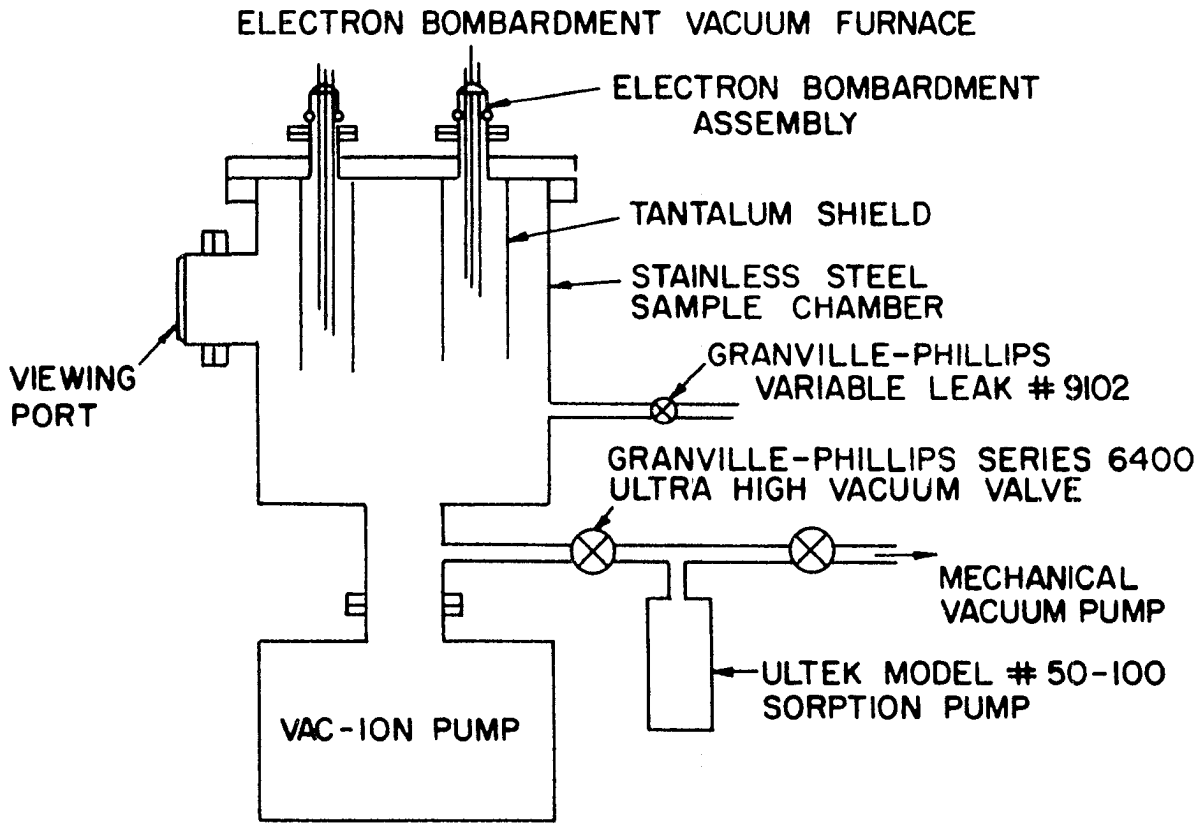

Figure 5. Electron bombardment vacuum furnace

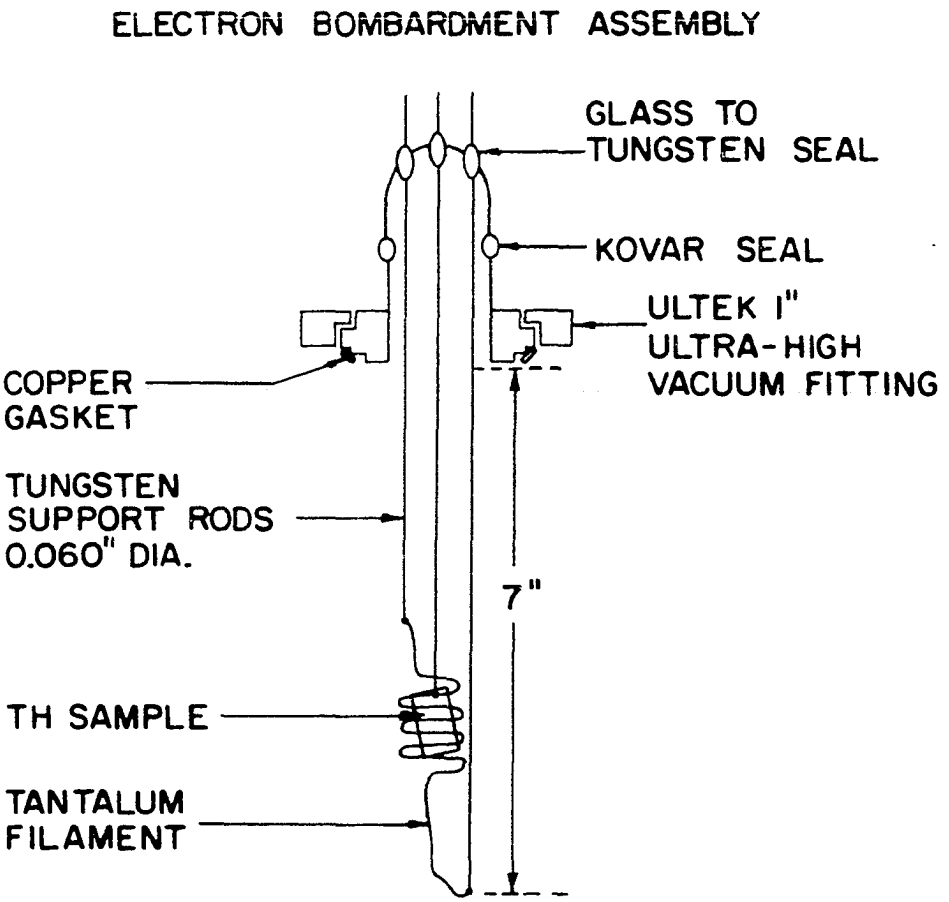

Figure 6. Electron bombardment assembly

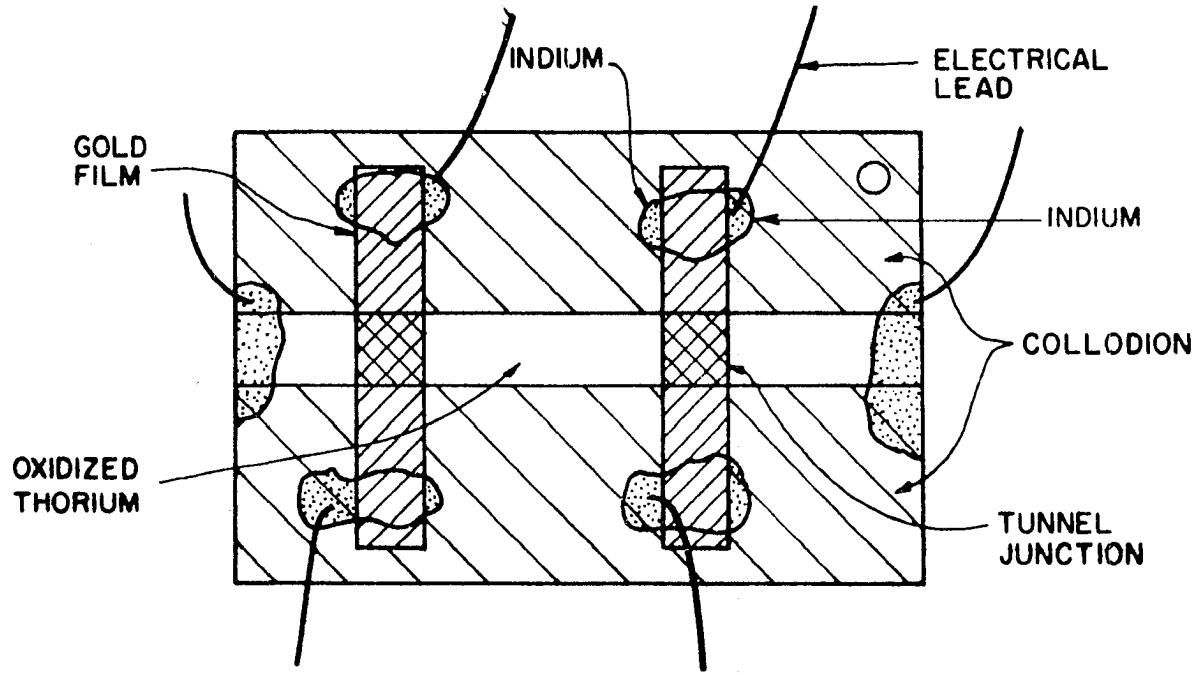

Figure 7. Illustrates two completed tunnel junctions

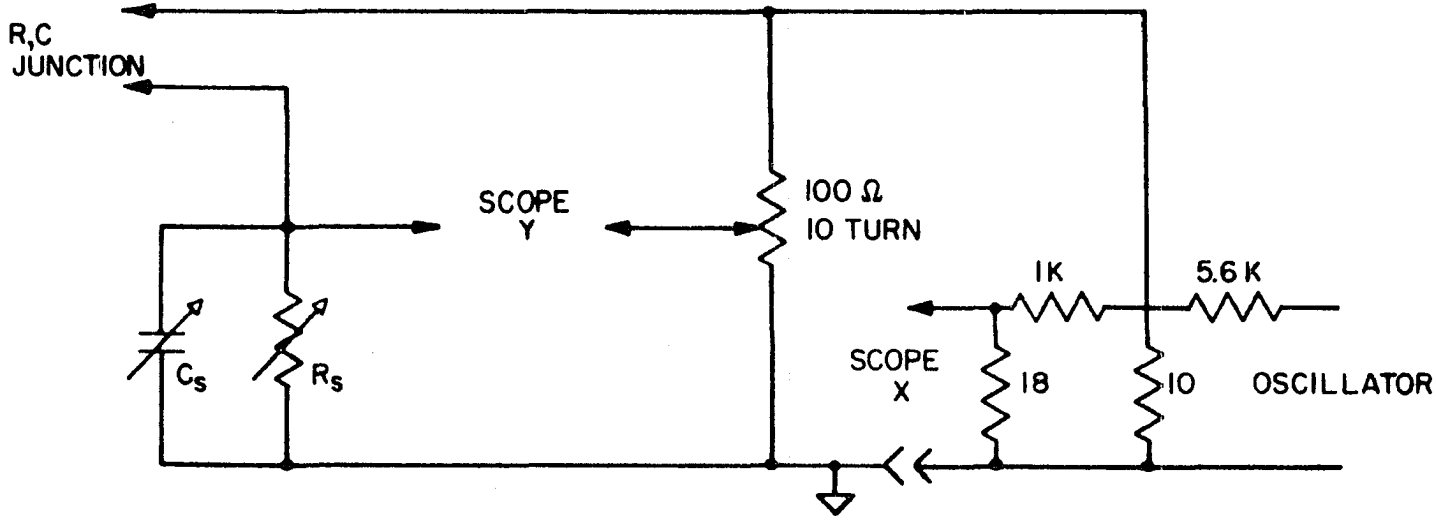

Figure 8. Bridge used to monitor tunnel junction resistances during evaporation

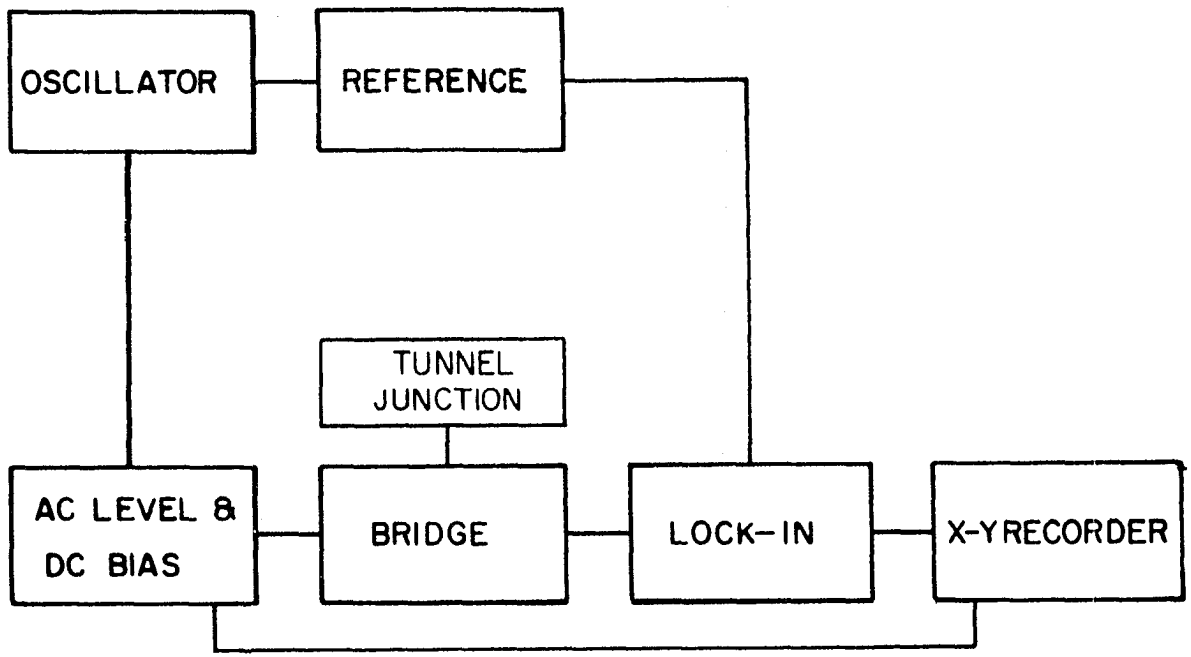

Figure 9. Block diagram of the electronic detection system

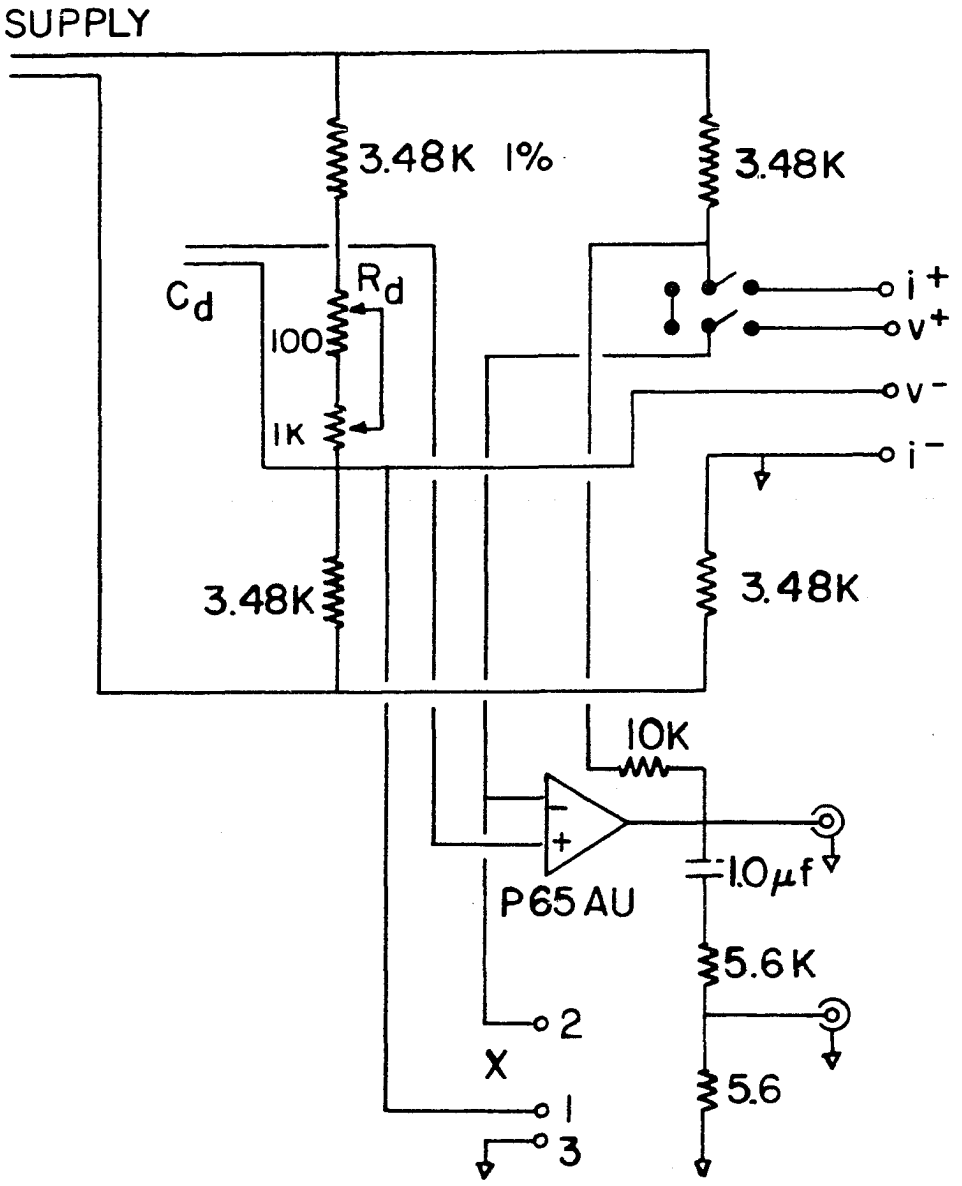

Figure 10. Electron tunneling bridge circuit

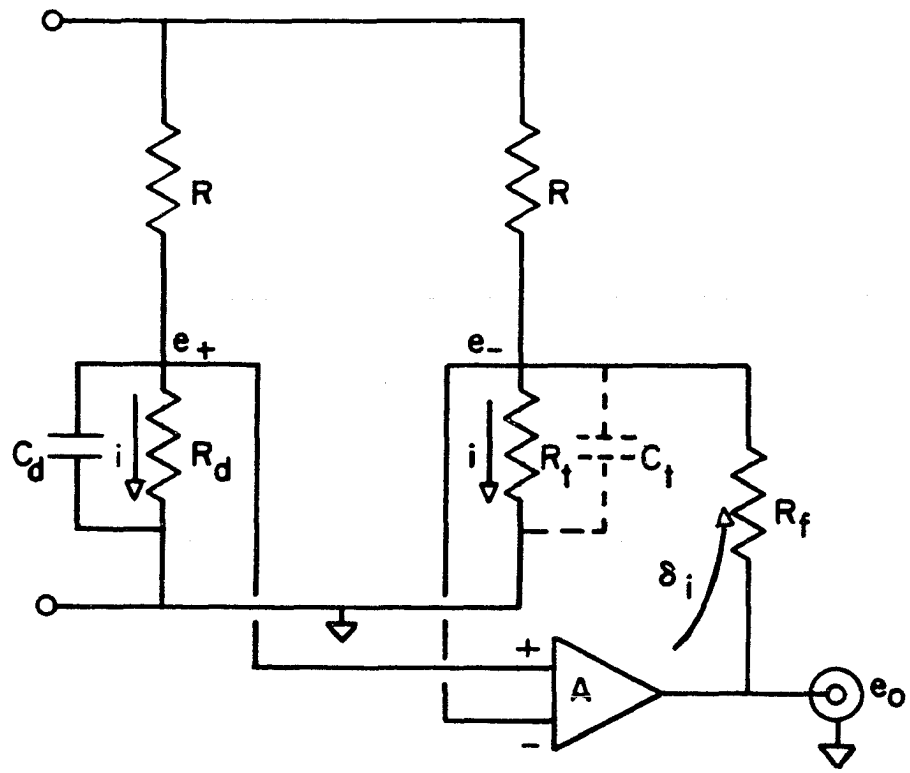

Figure 11. Simplified bridge circuit

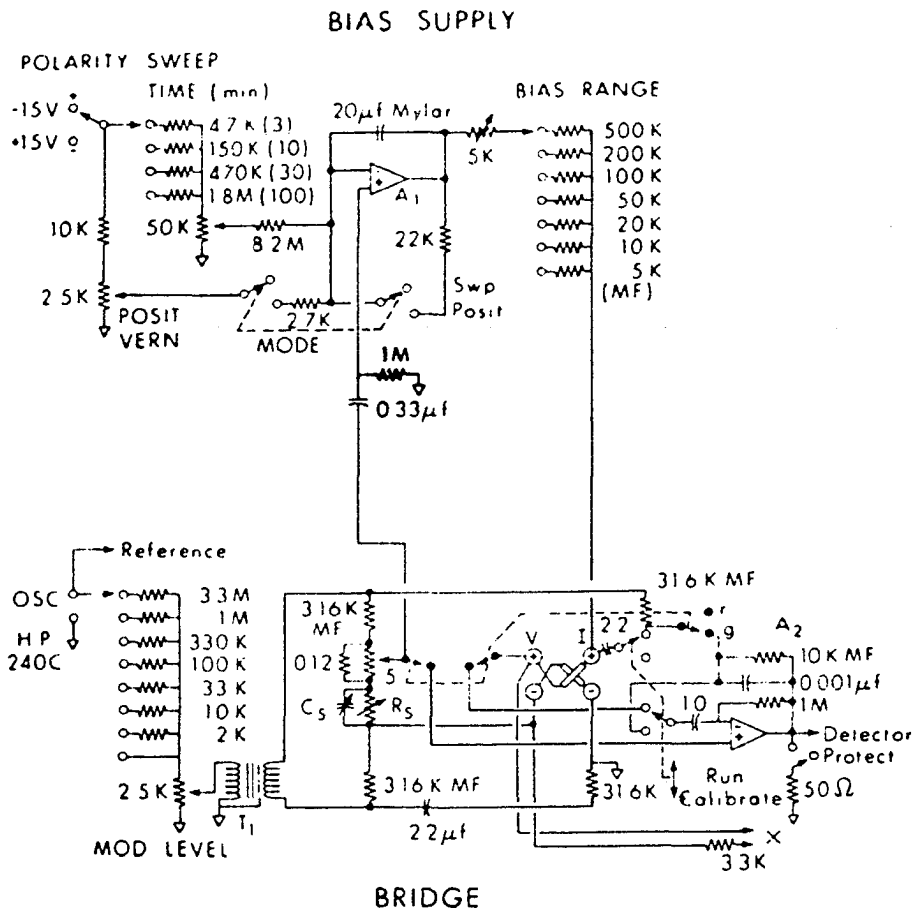

Figure 12. Electronic detection system

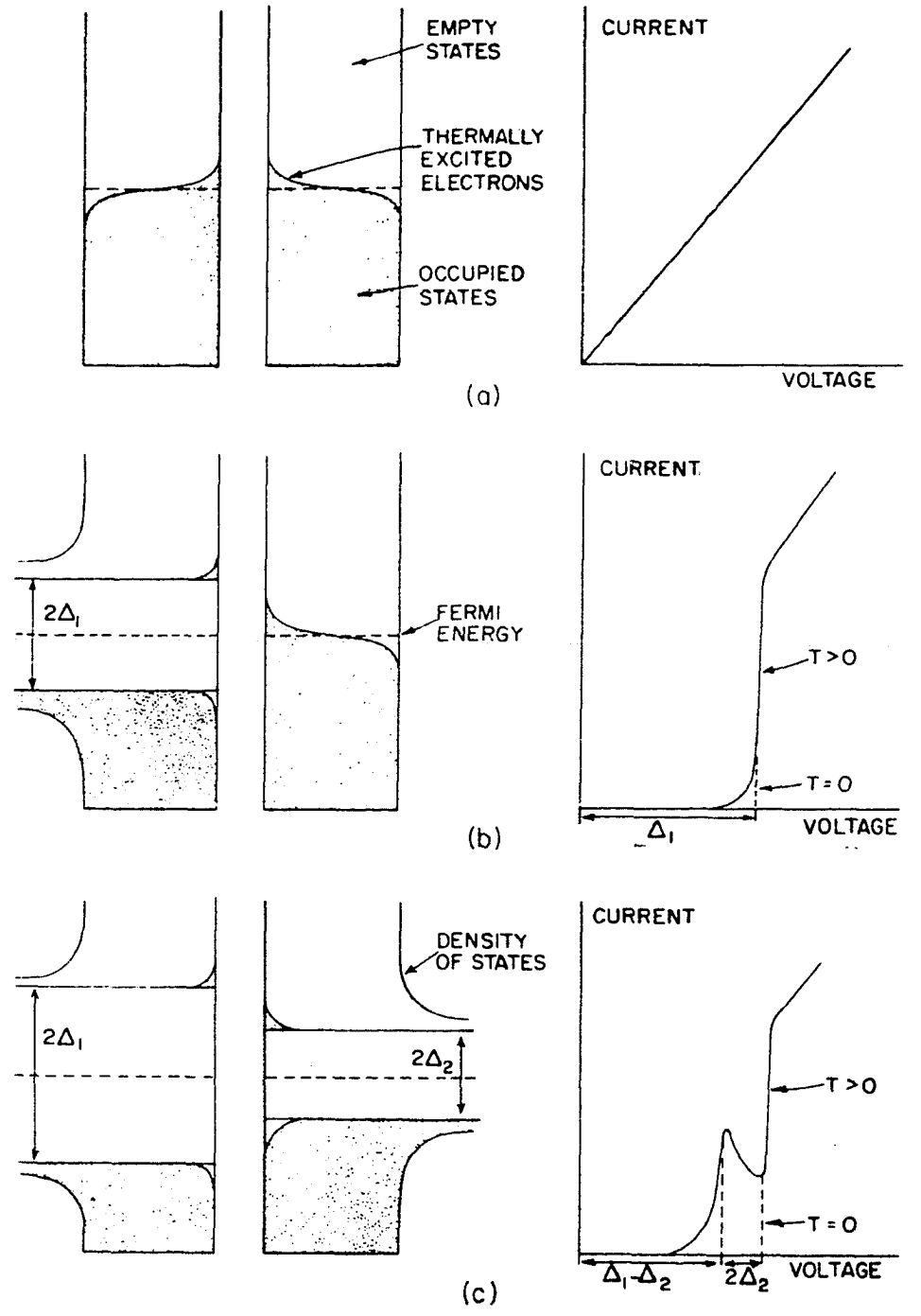

Figure 13. Energy diagram displaying the density of states and the current-voltage characteristics for three cases: (a) Both metals in the normal state; (b) One metal normal and one metal superconducting; (c) Both metals superconducting

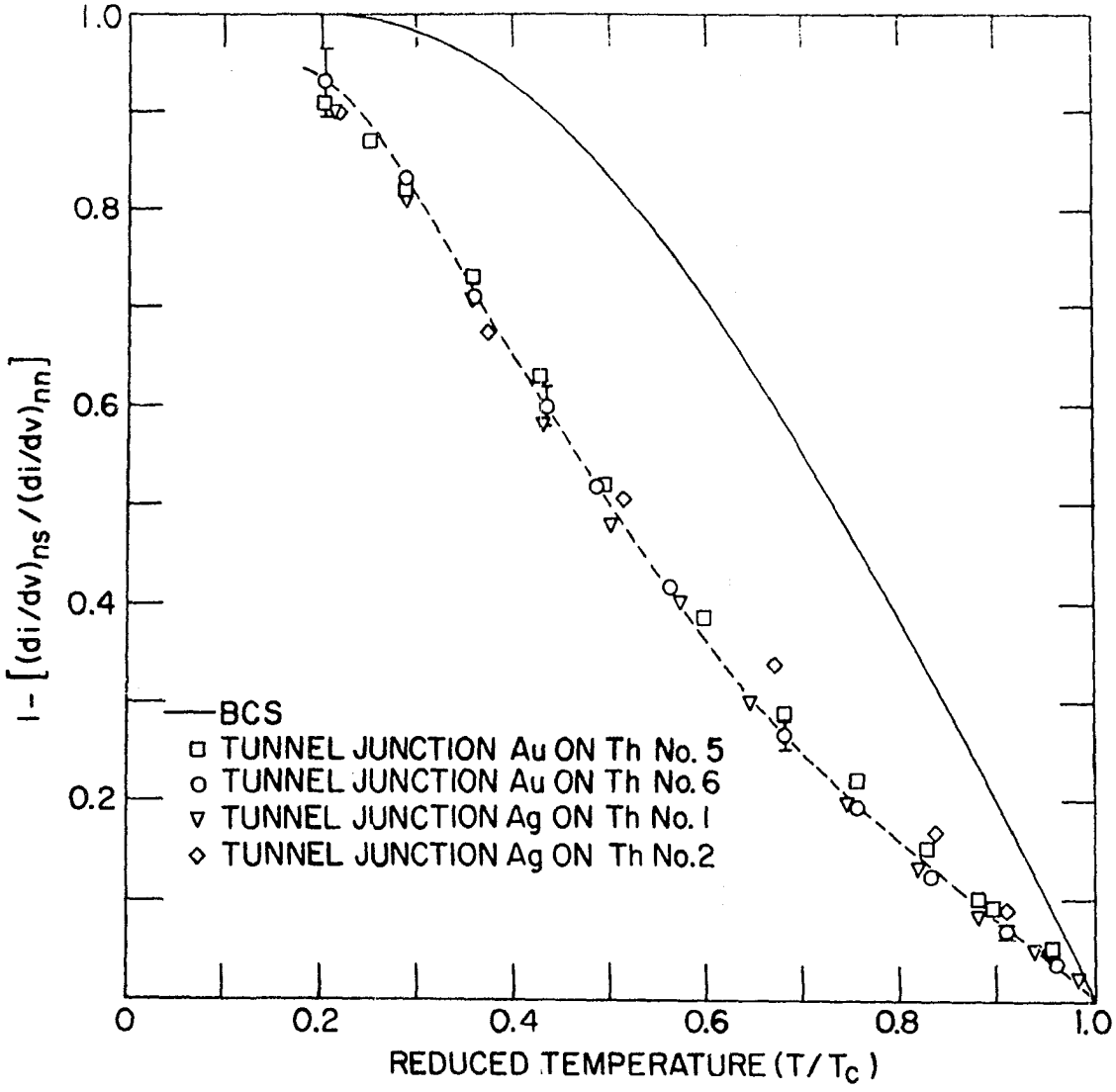

Figure 14. Temperature dependence of σ_o for the single crystal tunnel junctions

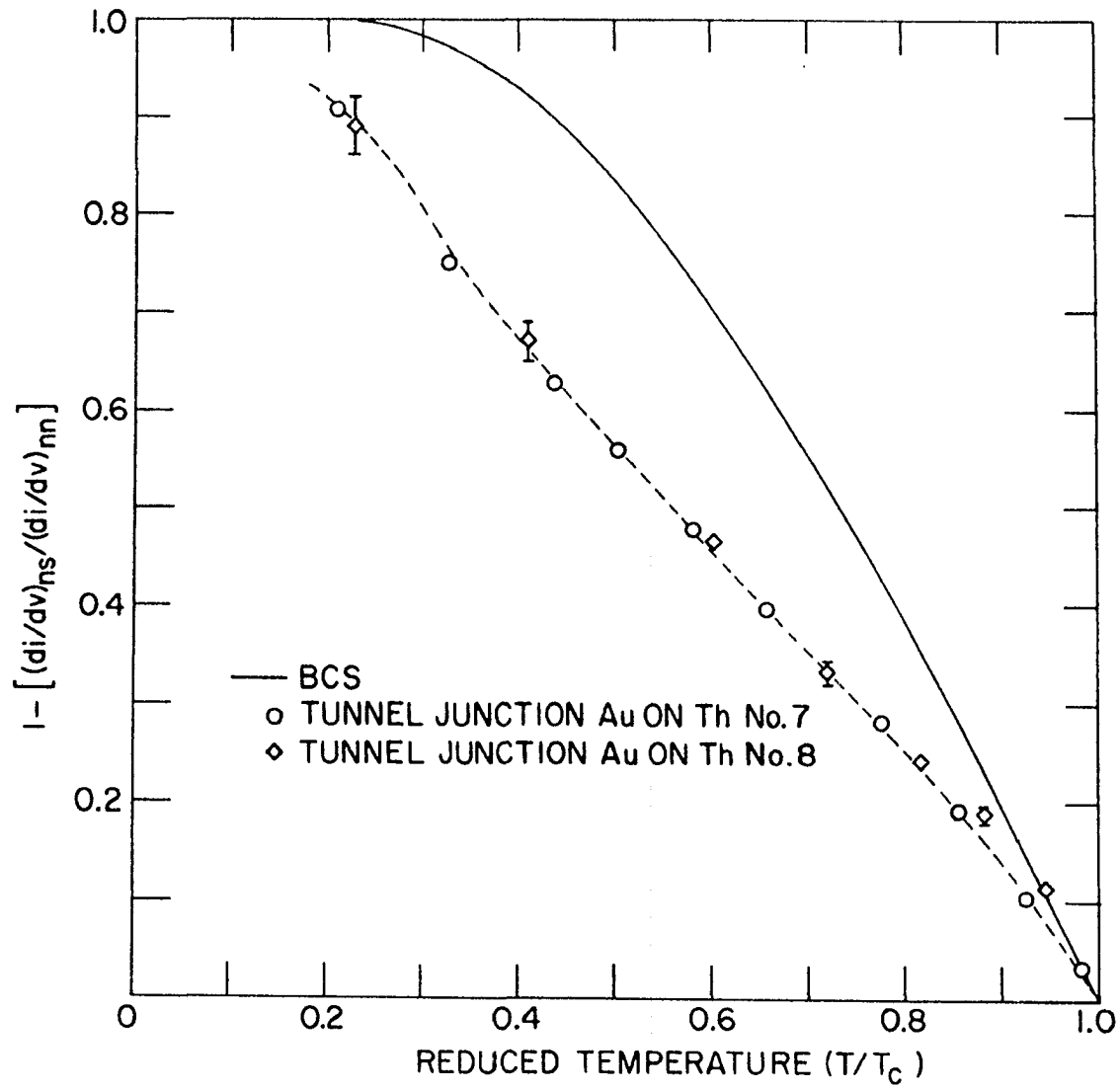

Figure 15. Temperature dependence of σ_o for the partially single crystal tunnel junctions

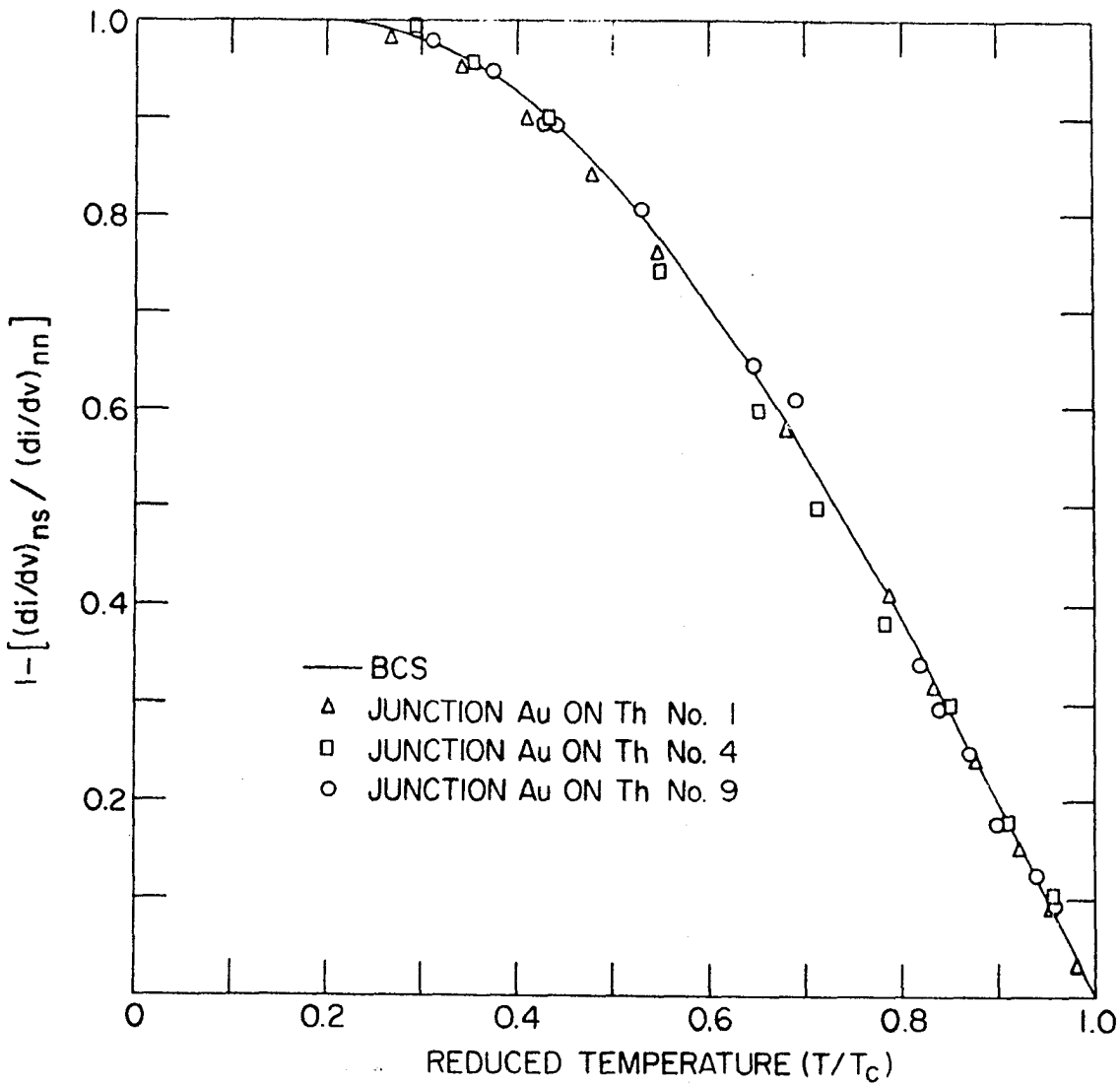

Figure 16. Temperature dependence of σ_o for the BCS-like tunnel junctions

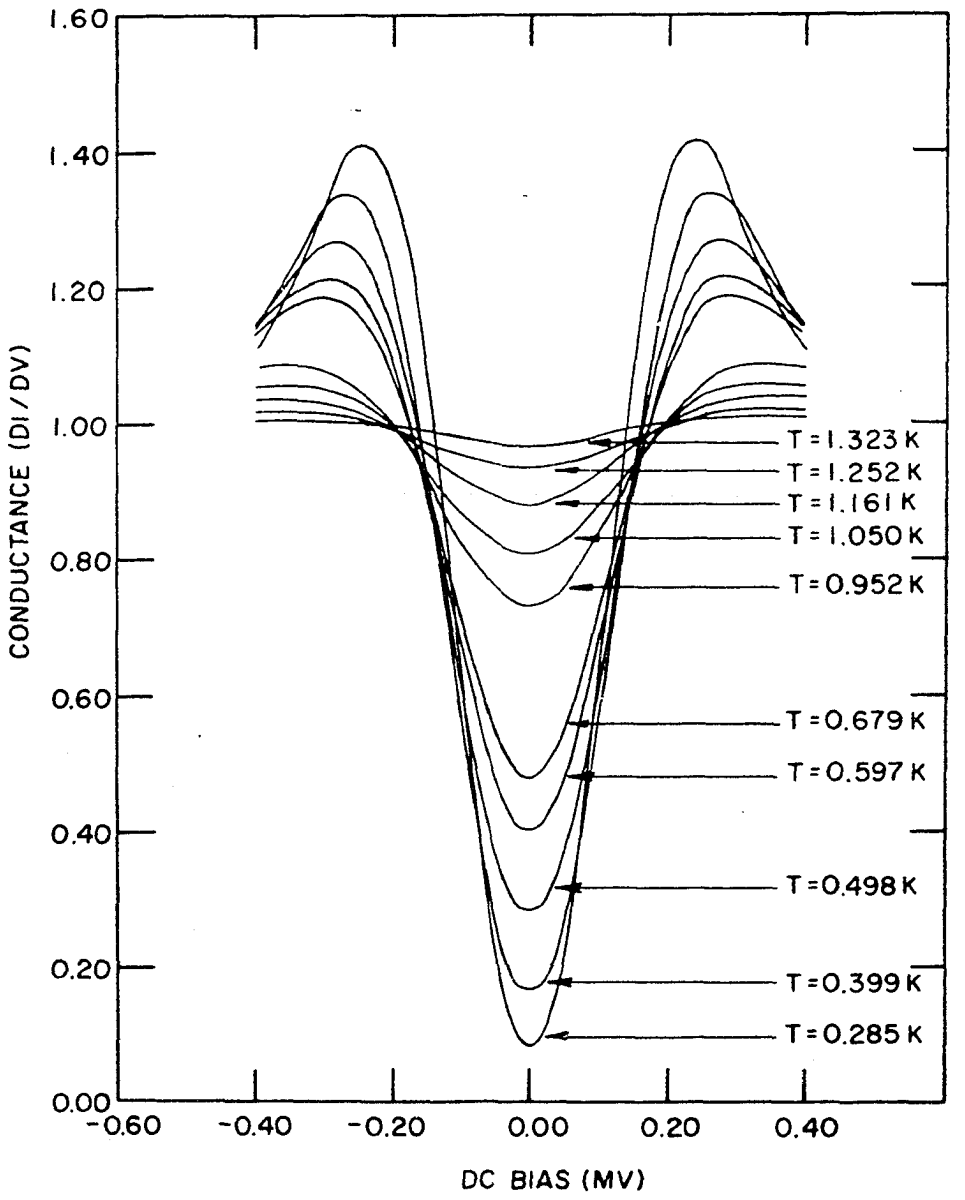

Figure 17. Normalized conductance curves for a single crystal tunnel junction (Au on Th No. 6)

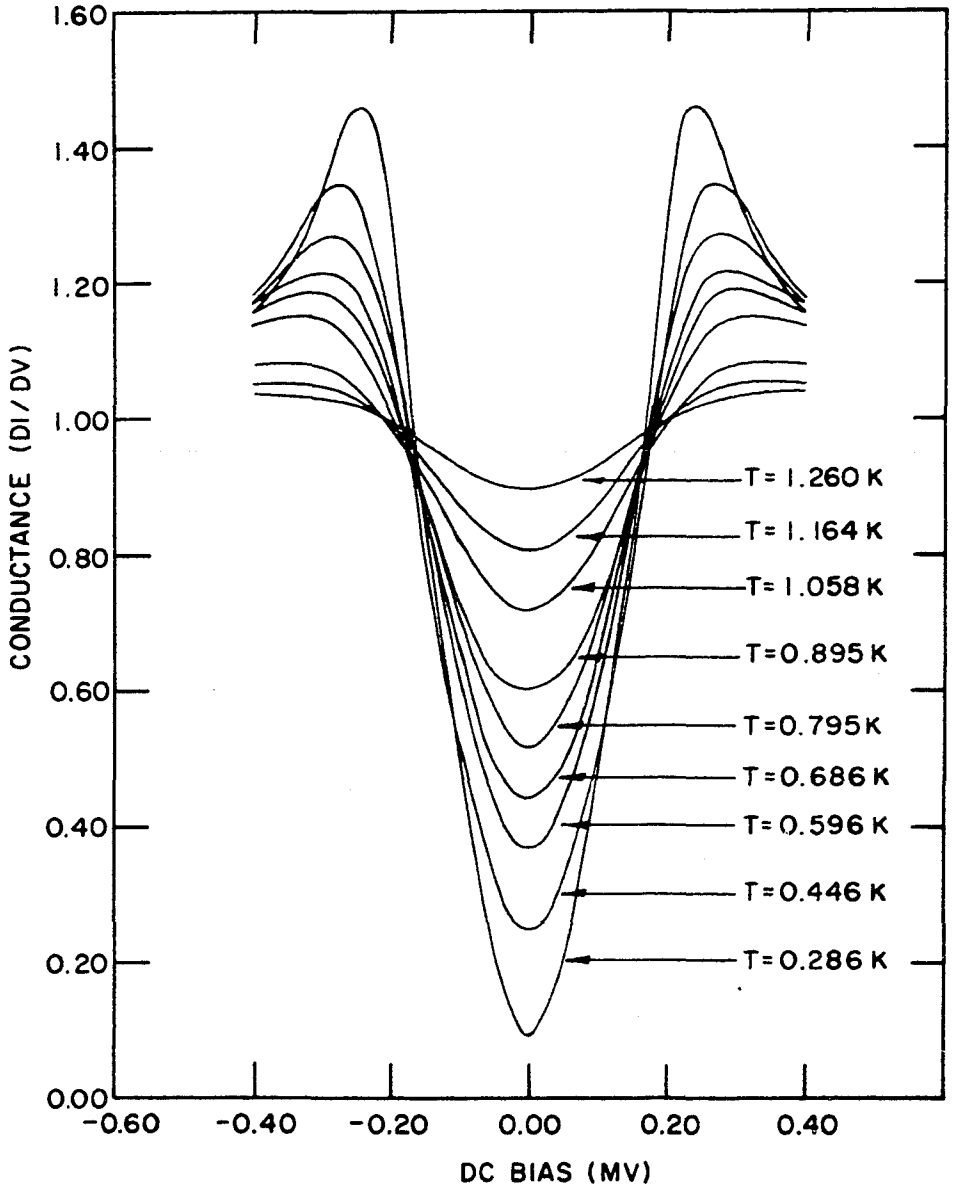

Figure 18. Normalized conductance curves for a partially single crystal tunnel junction (Au on Th No. 7)

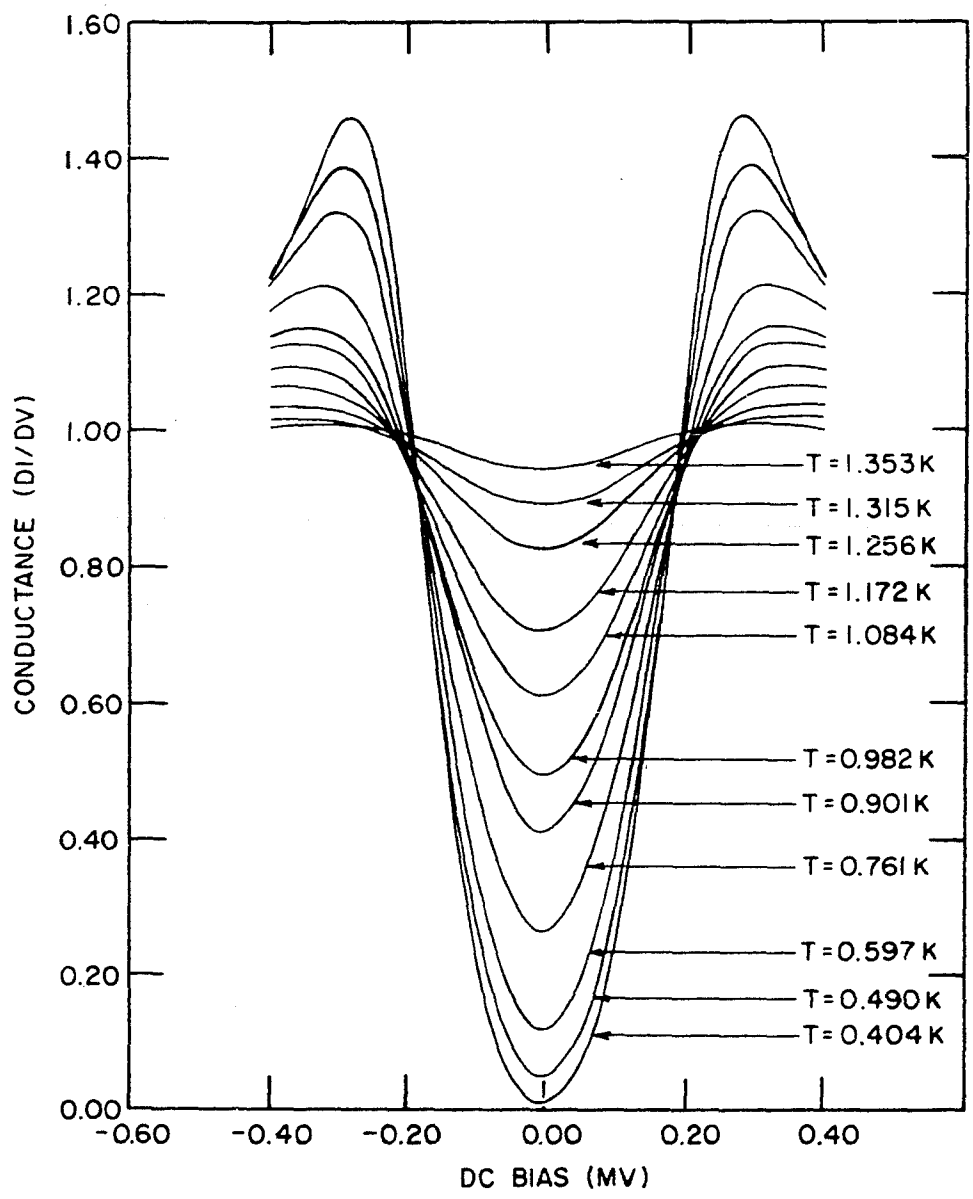

Figure 19. Normalized conductance curves for a BCS-like tunnel junction (Au on Th No. 4)

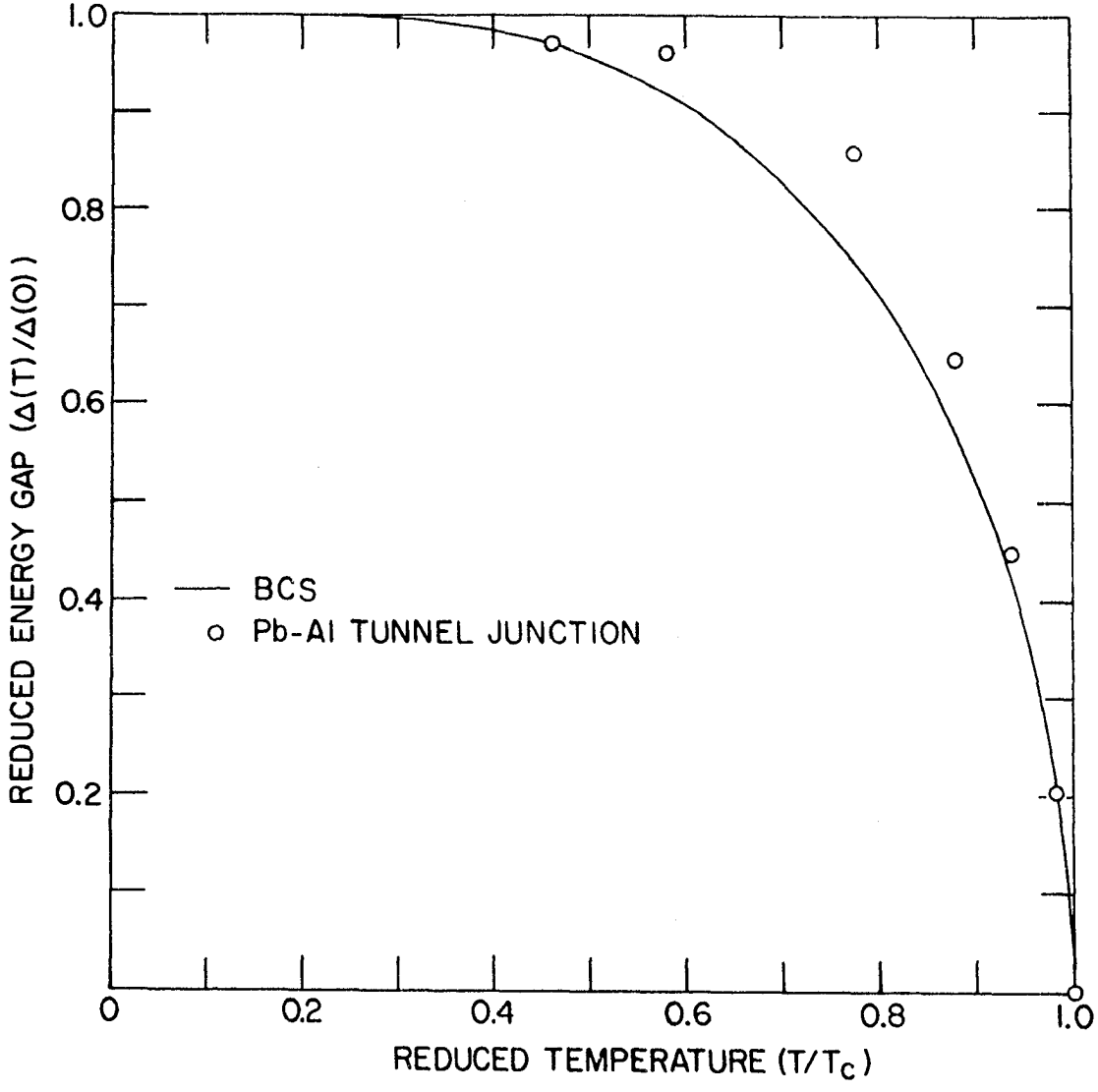

Figure 20. Energy gap data for aluminum

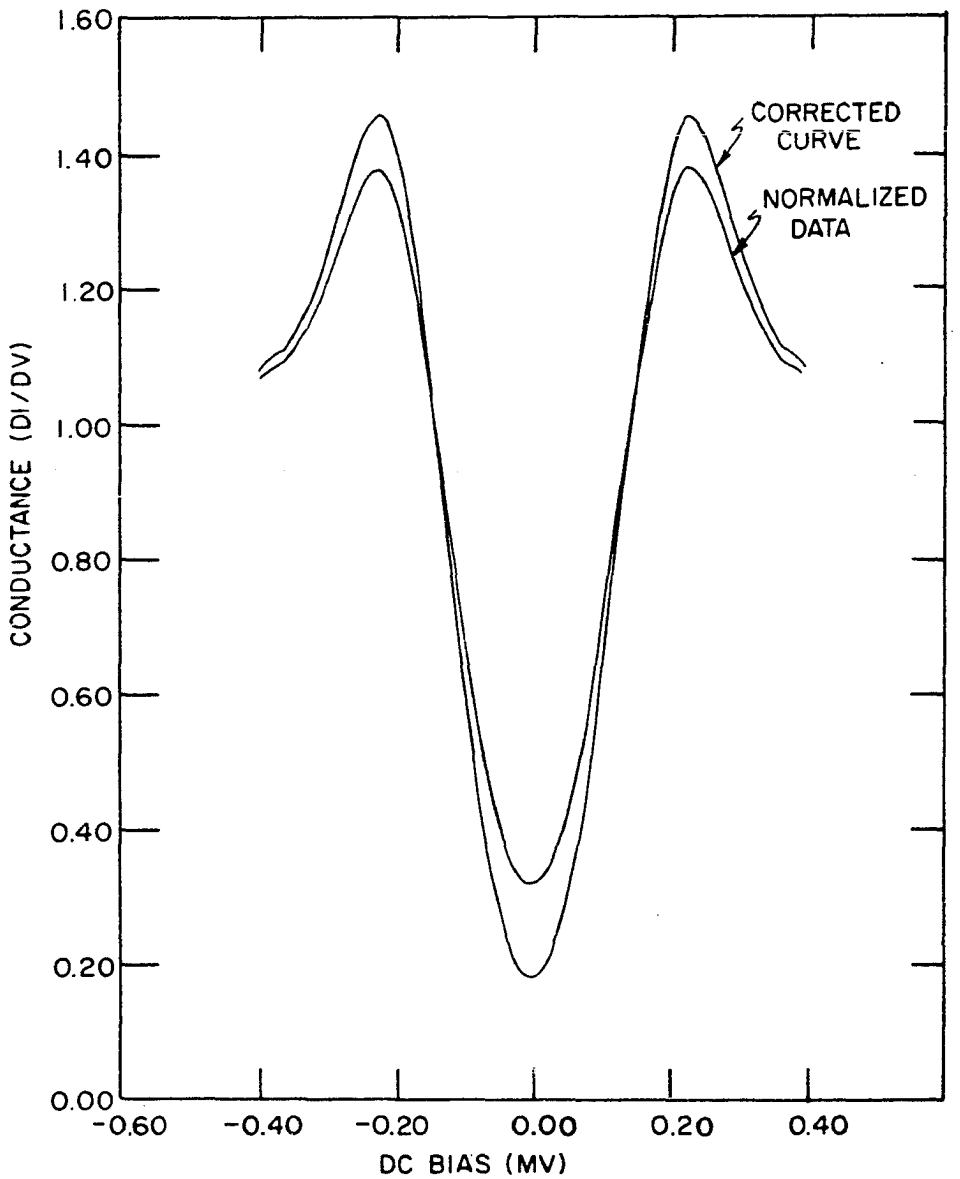

Figure 21. Illustrates the effect of the parallel conductance correction (Ag on Th No. 1, T = 0.384 K, $(di/dv)_{\parallel} = 0.168$)

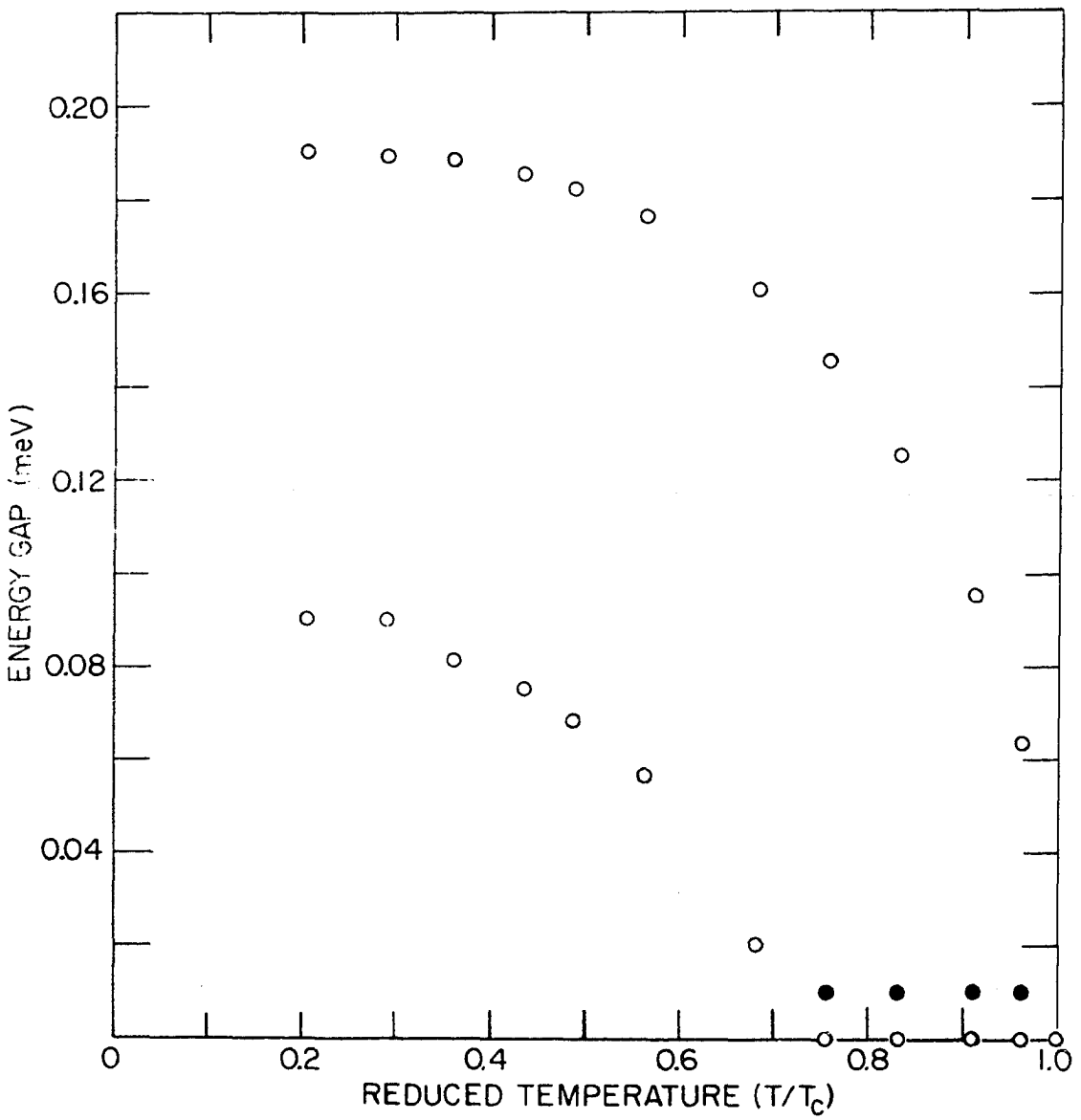

Figure 22. Energy gaps used to fit data for a single crystal tunnel junction (Au on Th No. 6)

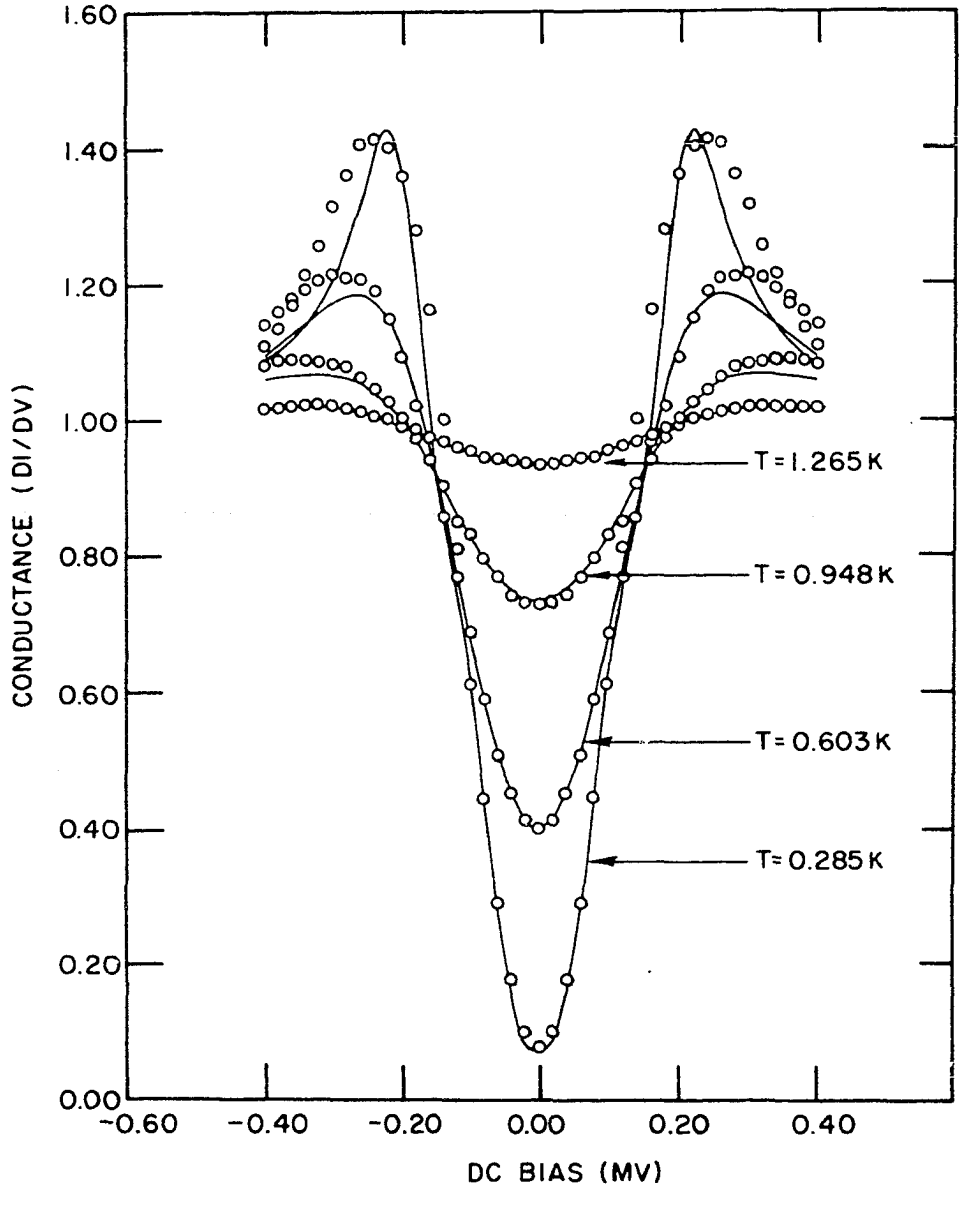

Figure 23. Comparison of the data (open circles) and the calculated curves for a single crystal tunnel junction (Au on Th No. 6)

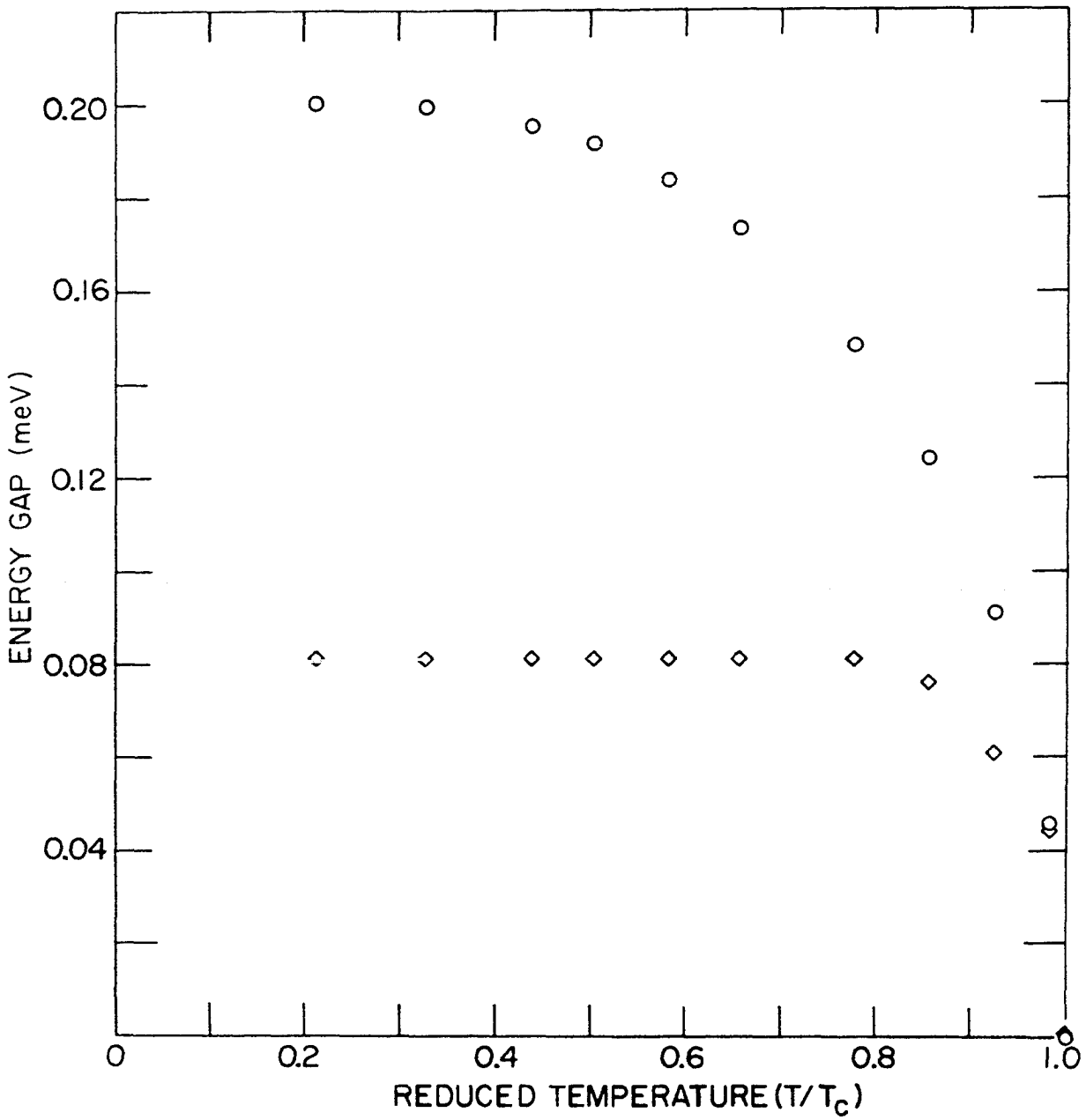

Figure 24. Energy gaps used to fit data for a partially single crystal tunnel junction (Au on Th No. 7)

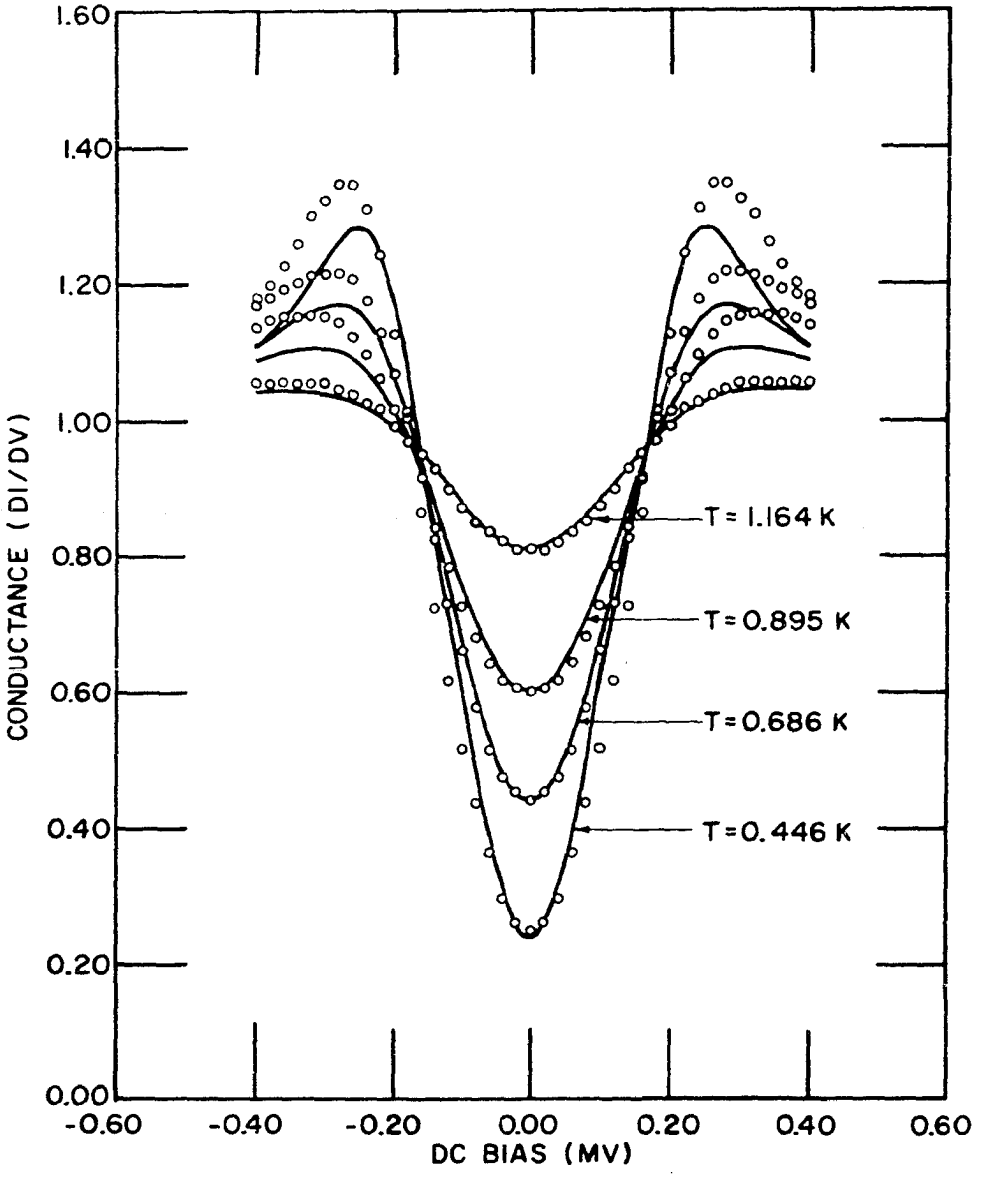

Figure 25. Comparison of the data (open circles) and the calculated curves for a partially single crystal tunnel junction (Au on Th No. 7)

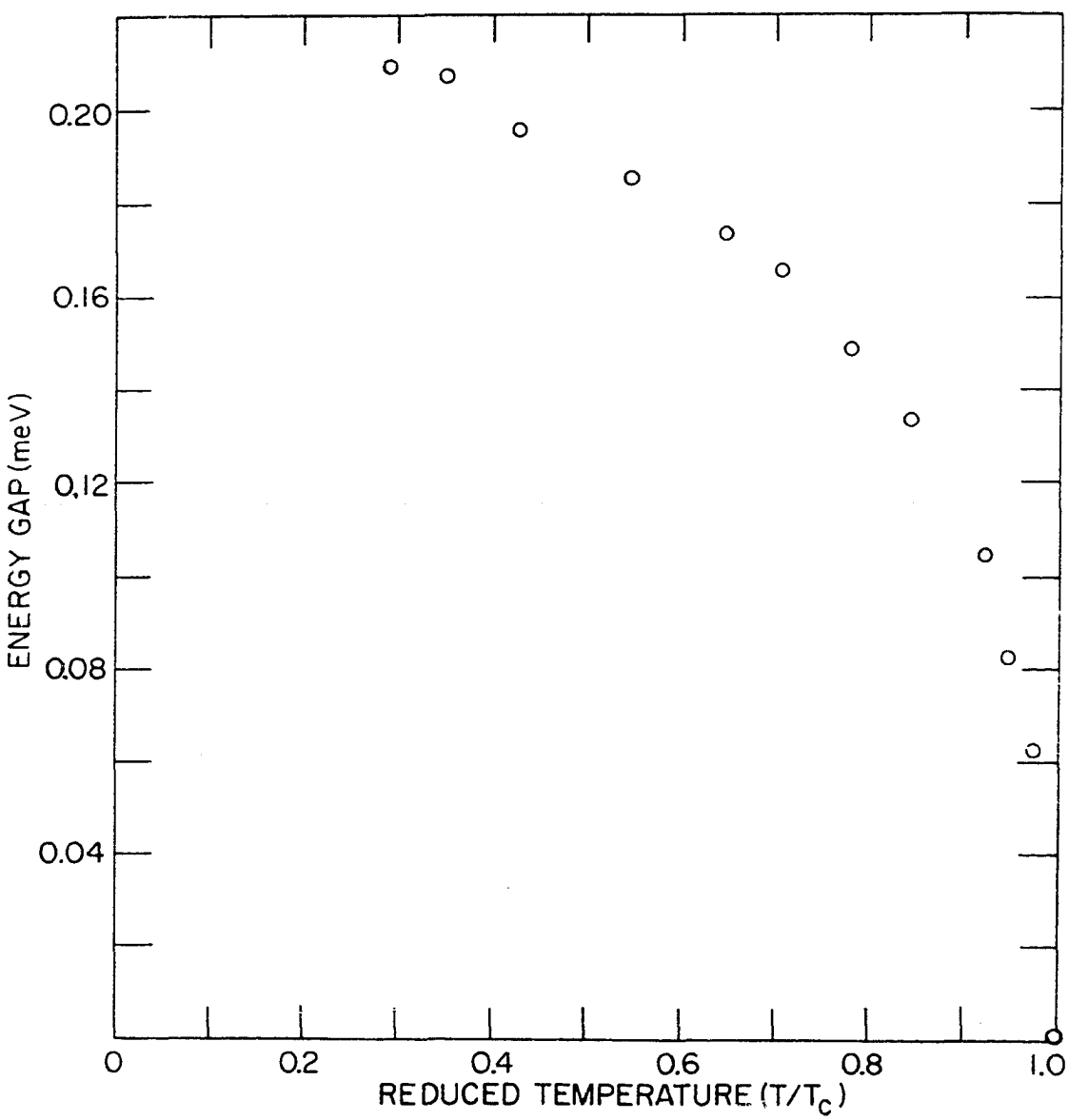

Figure 26. Energy gaps used to fit data for a BCS-like tunnel junction (Au on Th No. 4)

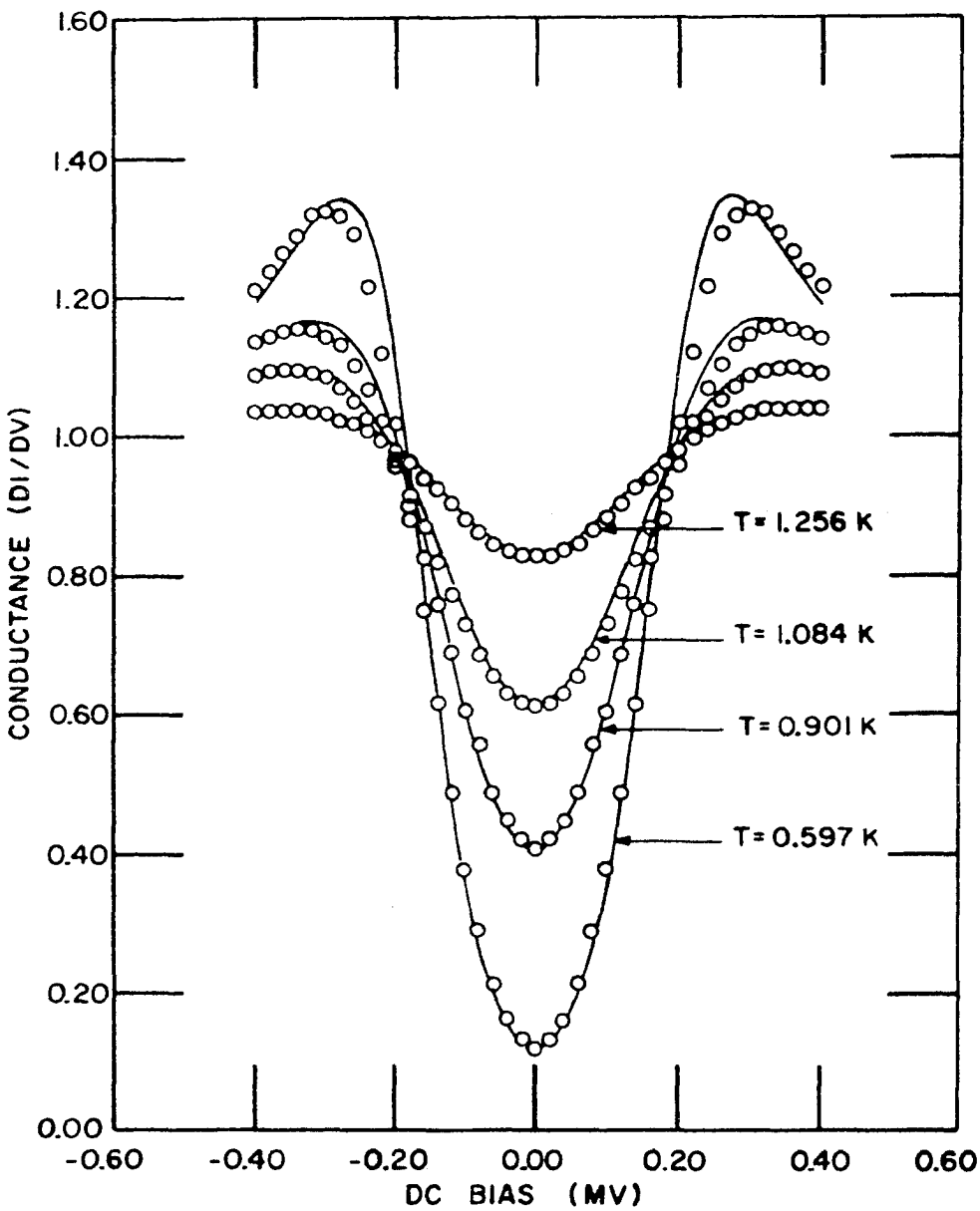

Figure 27. Comparison of the data (open circles) and the calculated curves for a BCS-like tunnel junction (Au on Th No. 4)

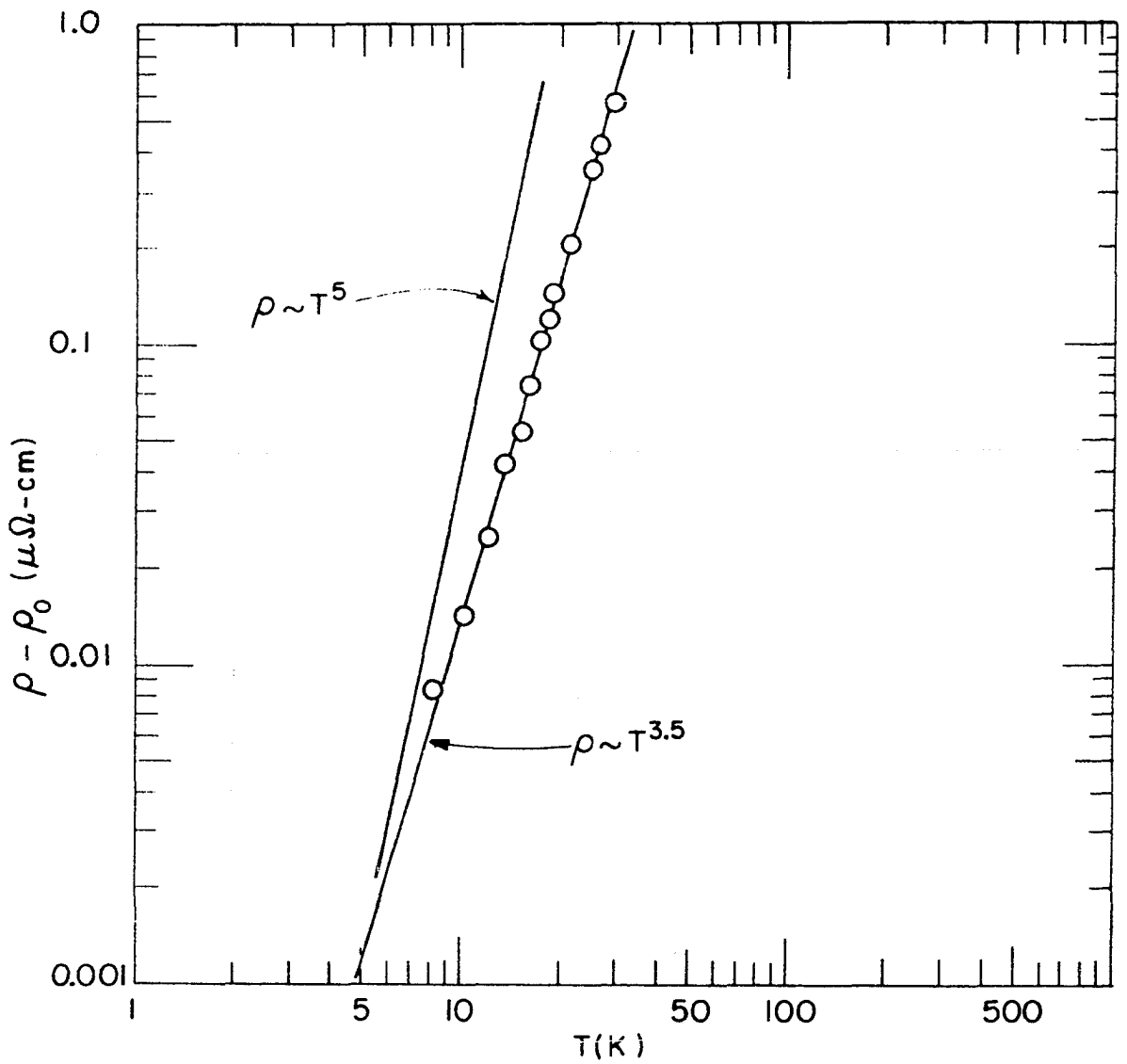

Figure 28. Low temperature resistivity of pure thorium